# PHOTONIC CRYSTAL ENHANCED MICROSCOPY FOR THE CHARACTERIZATION OF CELL ATTACHMENT

BY

ERICH ALEXANDER LIDSTONE

DISSERTATION

Submitted in partial fulfillment of the requirements
for the degree of Doctor of Philosophy in Bioengineering
in the Graduate College of the
University of Illinois at Urbana-Champaign, 2013

Urbana, Illinois

Doctoral Committee:

Professor Brian T. Cunningham, Chair
Professor Lawrence B. Schook
Professor Gabriel Popescu
Assistant Professor Gregory H. Underhill

# ABSTRACT

As basic science research has increased in both complexity and scale, so too has the importance of cost-effective and generalizable techniques for the interrogation of cells and tissues. Over the past several decades, several technologies have been leveraged to meet this demand, recently including photonic crystal (PC) biosensors. This work describes the application of PC biosensors to cell microscopy, resulting in a label-free imaging technique capable of measuring cell attachment and attachment modulation. The approach uses a photonic crystal optical resonator surface incorporated into conventional microplate wells and a microscope-based detection instrument that measures shifts in the resonant coupling conditions caused by localized changes in dielectric permittivity at the cell-sensor interface. Four model systems are demonstrated for studying cancer cells, primary cardiac muscle cells, and stem cells. Each experiments yielded information regarding cell attachment density without the use of potentially cytotoxic labels, enabling study of processes including growth, development, differentiation, and death in the same cells for periods lasting several days. After demonstrating this technology in several systems typical of cell biology problems, PC biosensors were applied toward the investigation of tumor immunity. In particular, it has remained difficult for immunologists to study how tumor cells interact with cells of the innate immune system, especially in the context of specific apoptotic recognition. The final chapter details the use of PC biosensors in detecting interactions between two distinct cell types, the reported use of label-free biosensors to detect such cellular changes.

# ACKNOWLEDGEMENTS

I give my greatest thanks to my adviser, Prof. Brian T. Cunningham, for providing me the opportunity to contribute toward this continually fascinating and rewarding work. His guidance and encouragement have been steadfast and strong forces for my progress over the past several years, and I look forward to a fruitful and friendly professional relationship over the years to come. I am truly grateful for my fellow graduate students in the Nano Sensors Group and collaborating groups for their thoughtful advice and encouragement, particularly Leo Chan, Sherine George, Vikram Chaudhery, Anja Kohl, Meng Lu, William Goldschlag, James Polans, Ji Sun Choi, Goutham Pattbiraman, James Heeres, and Timothy Flood for their work on label-free photonic crystal-based detection. I thank my committee members, Lawrence Schook, Gabriel Popescu, Brendan Harley, and Gregory Underhill for their support and contribution to my work. I would also like to acknowledge financial support from the U.S. Army Medical Research and Material Command (USAMRMC), the Telemedicine and Advanced Technology Research Center (TATRC, W81XWH0810701), as well as resources and support provided by the University of Illinois Center for Nanoscale Science and Technology (CNST) and the U.S. Army Engineering Research and Development Center, Construction Engineering Research Laboratory (ERDC-CERL). I am additionally grateful for the support of the National Science Foundation (NSF) Integrative Graduate Education and Research Traineeship (IGERT) in Cellular and Molecular Mechanics and BioNanotechnology (CMMB IGERT 0965918). Finally, I thank my mother, my father, my sister, and my family and friends for their unwavering support and encouragement throughout my academic career.

# Table of Contents

# CHAPTER 1 - INTRODUCTION

## 1.1 Cell Attachment in Growth, Development, and Disease

Cell attachment is achieved through the careful orchestration of a complex network of signaling pathways, vital throughout normal growth and development. Early in the development of multicellular organisms, individual cells possess fates that are largely predictable. In the model organism *C. elegans*, for example, the origin and complete developmental fate for every cell in the adult organism has been ascertained and reported [1-2]. As the size and scale of growth and development increase, however, this predetermined nature of fate gives way to more pragmatic, situation- and environment-driven fates. For an organism to survive, its cells must respond appropriately to dynamic and often unpredictable environmental stimuli. Moreover, the organism's survival mandates that a particular cell respond to stimuli in a fashion that is truly best for the organism as a whole – a representative example is that of apoptotic cell death that occurs in mammalian fetal hand plates to yield individual digits. Fetal cells must activate and respond to complex and variable signaling cascades to carry out these intricate processes; as a result, they alter their own makeup as well as their adhesions to neighboring cells and the ever-changing extracellular matrix (ECM). Without a capacity to assess and respond to the state of the local microenvironment including available nutrients, neighboring cells, and the ECM, a cell is unable to develop to its full potential, especially with respect to a greater host.

As much for normal growth and development, cell attachment, adhesion, and signaling play a critical role for cells engaged in pathogenic processes, critically exemplified by the acquired and abnormal metastatic qualities of malignant cancers [3-9]. In 2010, over 500,000 deaths occurred in the US as a result of uncontrolled cancer, approximately 90% of which can be attributed to metastatic disease [10-11]. Metastases are tumor implants that remain discontinuous with respect to the primary tumor [12]. Metastasis, referring to the translocation of a tumor to a distinct location, is a defining characteristic of malignant neoplasms. A hallmark of such malignancies is the ability to undergo epithelial to mesenchymal transition, allowing tumor cells to travel through and around natural barriers present throughout the body [13]. Another property common to malignant neoplasms is the ability to evade or inhibit natural defenses present in the innate and adaptive arms of the immune response. Many mechanisms have evolved to prevent

the uncontrolled proliferation of cells and pathogens within the body [14]. There are natural anatomical barriers and basement membranes, mucus- and immunoglobulin-secreting cells designed to elicit a response targeted against foreign invaders. There are complex pathways initiated upon the first encounter with a new challenge or the repeated recognition of a past disease [15-19]. These mechanisms, however, can be compromised in the case of cancer, as the threatening cells arise from the same lineage as those of the host organism; they are naturally better equipped to evade the immune response, and are indeed able to use their recognition as 'self' to prevent induction of the inflammatory response. Briefly, tumors growing in the body commonly initiate a process of immunoediting that continues to induce (1) cancer elimination; (2) cancer equilibrium, or immune selection of less immunogenic tumor cells; or (3) tumor escape, the uncontrolled growth and proliferation of a tumor variant capable of resisting immune destruction [20-21]. In characterizing the ability of a tumor to undergo these disease-inducing changes, it is necessary to determine the factors that may contribute to their progress or inhibit them from causing malignancy.

To be sure, cancer is a global health problem; the WHO forecasts the worldwide incidence of cancer will triple between 2000 and 2030 [22]. Cancer is appreciated as a multifaceted aggregate of diseases exhibiting substantial heterogeneity, complexity, and severity. Clinical researchers and academic scientists have learned much about a number of critical pathways and causal relationships leading to some of the most common and the most severe forms of the disease, often with the aid of specific and sensitive detection tools including sequencing, fluorescence microscopy, flow cytometry [23-29]. While such methods have provided great insight by allowing researchers to study specific pathways, the specific assessment and analysis of cell attachment and morphology have only recently become accessible with the development of low-throughput techniques including single molecule and atomic force microscopy, total internal reflection fluorescence microscopy, and optical tweezers [30-36]. Researchers have been actively pursuing newer, less expensive, and higher-throughput options for the general assessment and characterization of cell attachment [37-39]. The possibility of such tools holds great promise; detailed knowledge of processes involved in pathogenic cell attachment will enable general, morphological studies of the mechanisms underlying cancer cell growth and metastasis. Moreover, the capacity of instrumentation used to gain this information will allow exploration of the factors by which tumor cells undergo epithelial-mesenchymal transition and migration, processes central to metastatic disease [40]. Detailed knowledge of these processes will allow mitigation of would be metastatic cells through either

prevention or intervention [41-42]. Such advancements would also be instrumental in defining the characteristics responsible for preventing the body's immunological defenses from responding quickly and effectively to nascent tumors [43]. Finally, increased awareness of stem cell attachment and the factors which encourage differentiation down desired lineages will allow optimization of culture techniques and niche design to encourage healing and prevent metastatic growth [41, 44-46].

To understand these critical processes at a level allowing their manipulation and management, it is necessary to develop tools and technologies that will enable life science researchers to interrogate them effectively and efficiently. The study and characterization of these processes has relied primarily on general immunohistological and specific fluorescent staining techniques. Such experiments enabled life science researchers to pinpoint and explain processes of vast biological and medical interest, ranging from disease detection to disease therapeutics. These assays, however, have relied heavily on the use of costly stains, fluorophores, and enzymes that are often difficult to procure and characterize. Moreover, the reagents used for the investigation of a specific biological problem are frequently of limited use beyond the scope of the aforementioned problem. Recently, many advances have been made in the field of label-free sensors, designed for to illicit similar or complementary information without the need for specific markers. In this work, recently developed biosensors known as photonic crystals are demonstrated as a modality for the quantification and imaging of cell attachment and adhesion as well as imaging how cell attachment changes in the context of cancer immunosurveillance.

## 1.2 Label-Free Cell Attachment Imaging

Several optical and electrical techniques have been employed to interrogate cells in the absence of potentially cytotoxic or complicating fluorophores and stains, including surface plasmon resonance (SPR), impedance imaging, interference microscopy, and photonic crystal (PC) biosensors [47-50]. Each of these imaging techniques has been demonstrated as capable of imaging cells in the absence of specific markers or stains, proving their utility for the characterization of analytes according to changes within the samples in lieu of being relayed through a series of potentially variable biochemical binding interactions. Though the following label-free approaches differ from one another in fundamental mechanism, each makes use of a transducer to convert physical alterations in a given analyte into a detectable signal, such as a change in electrical impedance or a shift in phase or wavelength. Each modality has a unique combination of advantages, lending it distinct capabilities and limitations.

*Surface Plasmon Resonance Imaging*

Surface plasmon resonance (SPR) is a chemical detection technique that has been used for the detection of target molecule binding and affinity [51]. Briefly, SPR optical sensors are made up of an optical system, a transducing medium relating the optical domain to the chemical/sensing region, and an electronic system to support the sensor and to allow data processing, collection, and analysis (Figure 1). The transducing medium transforms changes that take place in the sensing region into changes in refractive index. The optical part of the sensor contains a source of illumination and an optical structure in which surface plasmon waves are excited and interrogated. During interrogation, the sensor generates an electronic signal to be processed by the electronic system. To interrogate the sensor, light is directed via a waveguide into a metal layer built into the sensor and interacting directly with the analyte. Changes in the analyte alter the refractive index within the sensing region, causing a change in the sensor response. Commonly used approaches for detecting SPR signal include measurement of the optical wave intensity near the resonant condition and measurement of the resonant condition using either angular or wavelength-based interrogation techniques [52-55]. From 1987-1988, Yeatman and Ash documented the first use of SPR instrumentation capable of imaging over a given sensor area [56-57]. After the invention of surface plasmon resonance imaging (SPRI), its first application was toward the characterization of thin biomolecular films [58].

Over the past twenty years, improvements in instrument design have yielded several configurations, the latest of which are capable of imaging individual cells on a range of ECM substrates [39]. While SPRI remains useful for the characterization of cell:matrix adhesion density, its utility is somewhat compromised by its reliance on costly materials. The flow-cell format is subject to the accumulation of larger aggregating molecules, and sufficient removal is often impossible, necessitating costly replacement of the chip to achieve true reproducibility [51, 59-60]. The increased cost of SPR for detection of cell attachment therefore presents challenges that may be addressed with alternative optical biosensor instrumentation.

*Electrical Impedance Spectroscopy Imaging*

Another modality, which has seen recent success in cellular imaging, is that of electrical impedance spectroscopy (EIS). EIS is based upon the principle of applying differential voltage to an electrode to monitor changes in the current response. Processes such as biochemical binding events and cellular apoptosis have been demonstrated to elicit detectable changes in impedance in the absence of specific labels or stains [61]. EIS has indeed been used to study cell process ranging from spreading and adhesion to motility and invasion [62-63]. Until recently, however, imaging with EIS has not been an accessible undertaking. The dimensions of conveniently manufactured electrodes have historically been the limiting factor with regard to the spatial resolution of EIS imaging. Simply put, a complex array of microelectrodes will be subject to complex interference and decreased impedance signal per microelectrode. As a result, it has not been possible to image changes in electrical impedance on the order of single cells using such a configuration.

Recently, however, Wang and colleagues have developed a method that combines the impedance capabilities of EIS with the enhanced resolution of SPR imaging [64](Figure 2). The new technique is known as Electron Impedance Microscopy, and relies on the sensitivity of SPR to detect changes in surface charge density. As this information can be collected optically, it is possible to do so with a high temporal resolution, and with spatial resolution sufficient to image individual cells. Due to the high temporal resolution, it is possible to capture phenomena that are short-lived, as in the case of electroporation demonstrated by Wang et al. As the technology relies on SPR-compatible materials,

however, it is subject to some of the same cost constraints. As materials and supporting equipment become more widespread, however, this could change.

*Spatial Light Interference Microscopy*

Another technique available for studying changes in cell morphology and structure is that of Spatial Light Interference Microscopy (SLIM). Although used earlier for characterization of nanostructures, Wang et al. first demonstrated use of the technology for use in cell biology experiments in 2011 [65-66]. SLIM effectively combines elements of classical phase-contrast microscopy with those of holography, in which phase information is recorded. In short, the resulting technique allows collection of optical path length and phase shift data across and through transparent samples (Figure 3). The resulting images provide information that is typically difficult to observe with phase-contrast and traditional fluorescence microscopy, and with a resolution that improves upon traditional phase contrast microscopy while eliminating certain problems including the common halo artifact. Moreover, the new microscopy technique is able to deliver morphological information about certain cell types, including the state of actin polymerization within growing neurofilaments. Because the technique can be applied flexibly, it is capable in multimodal imaging scenarios as well, allowing both specific fluorescent labeling and general optical path length quantification to be performed on a single sample in near real-time. Because the technique images through the entire sample, however, it may be difficult to parse out information relating specifically to cell attachment near the cell:substrate interface.

*Photonic Crystal Biosensors*

Photonic crystal biosensors are another recent addition to the array of tools used to study cellular and biochemical interactions in the absence of chemical labels or stains [67-68]. Photonic crystal (PC) surfaces can be designed to possess optical resonances known as guided-mode resonances [69]. Such resonances are present in optically permeable diffraction grating structures in which the period of refraction index modulation is smaller than the wavelength used for illumination of the structure. For guided mode resonance, modes diffract in both transmitted and reflected directions. Importantly, the reflected wave remains out of phase with the transmitted $0^{th}$ order mode by 180°, allowing for highly efficient destructive interference for transmitted light. In the far-field, this phenomenon can be observed

as a significant dip in transmission for illumination wavelengths and angles that satisfy the resonance condition:

$$\frac{2\pi}{\lambda}\sin(\theta) \pm m\frac{2\pi}{\Lambda} = \beta$$

where $\lambda$ is the wavelength of incident light, $\theta$ is the angle of illumination, m is the diffraction order, $\Lambda$ is the period of the structure, and $\beta$ is the real part of the propagation constant of the guided mode [70]. The resonance of the structure is important for label-free detection because the electric field generated by the illuminated device extends into the analyte and containing medium (typically air or water). As a result, physical changes occurring within an analyte can relate to changes in how the diffraction grating interacts with incident light, allowing transduction of the physical change into a detectable quantity.

The possibility of using PC biosensors to detect such changes has been successfully demonstrated for in a number of settings, often in the context of biochemical detection and characterization. The PC biosensors used in these studies are photoreplica-molded low-refractive index (RI) plastic subwavelength structure (SWS) diffraction gratings coated with a high-RI $TiO_2$ layer [71]. When white light illuminates the bottom of a sensor, a narrow band (resonant wavelength) of light is reflected at a normal angle [72]. Adsorption or attachment of material to the sensor within an evanescent field region results in a proportional change in the dielectric permittivity of the sensor, resulting in a shift of the resonant condition over the affected portion of the PC biosensor and effectively allowing quantification of mass-density changes on the sensor surface [67, 73]. The resonant condition can be assessed through monitoring of either the reflected band wavelength, maintaining a constant angle, or through observation of the resonant angle, maintaining a fixed illumination wavelength. Recent development of PC biosensor technology by Cunningham, Block, and colleagues has yielded the development of several PC-based sensing instruments, including a high-speed, low-resolution microplate-compatible, wavelength-based reader (BIND, SRU Biosystems) as well as a high-resolution, angle-based microscope capable of imaging individual microarray spots measuring tens of microns in diameter [67,74]. This combination of imaging setups allows both kinetic and high-spatial resolution studies to be performed over extended intervals, both of which provide unique advantages for particular applications.

While SPR and impedance techniques benefit from being a direct assay for physical change in the system studied, photonic crystal biosensors provide several unique and compelling advantages. PC biosensors are capable of near diffraction-limited imaging resolution due to the tight confinement of propagating photons, a property that remains an active challenge for SPR-based imaging [75-76]. Finally, the photoreplica molding process used for PC biosensor fabrication allows the construction of large, uniform at limited cost [26][41]. As PC biosensor imaging remains a fundamentally widefield technique, adoption of the technology to a CCD-compatible imaging setup was a relatively facile process, limiting the complexity of data interpretation and analysis. Because both high-throughput and high-resolution PC biosensor instrumentations are the focus of this work, the use of these technologies for studying cell attachment density and cell-cell signaling in the context of apoptotic recognition will be discussed at length in the remaining chapters.

## 1.3 Cancer, Tumor Immunity, and Cell Attachment

Tumor cells have been widely demonstrated to possess limited immunogenicity [77-78]. Historically, this has been attributed to the self-like qualities possessed by many tumor antigens – this reasoning, however, does not explain significant decreases in productive immunogenicity possessed by many transformed tumors [79-80]. Possible explanations for this incongruity have been extensively researched, resulting in several hypotheses engaging the concept of immunosuppressive activity exerted by tumor cells. The concept of immune editing refers to alterations in immune function that result from specific and cell-based interactions between a nascent tumor and the host immune defense [81]. Examples of tumor-derived effects on the immune system include the production of soluble factors including inflammatory mediators, cytokines, growth factors, and other signaling molecules capable of interfering with or circumventing the immune system [82-86]. In addition to these soluble factors, tumors necessarily induce changes in the surrounding ECM that can exert profound effects on cells throughout the local tissue [87]. Of particular interest are changes induce apoptosis or apoptotic signaling in the surrounding tissue, which has been shown to suppress the immune response through several mechanisms [88].

Recent work has demonstrated that apoptotic immunity influences tolerance to tumor antigen as summarized. In a phenomenon referred to as apoptotic recognition, tissue macrophages recognize apoptotic residues expressed on surrounding cells, and subsequently alter their response to cells expressing those residues. This alteration can include generalized or specific immunosuppression, effectively shaping the outcome of the eventual immune response. Briefly, exposure of primary macrophages to apoptotic tumor cells results has been shown to effect profound reduction in their immune response as characterized by the secretion of interleukin-2, a marker associated with T cell activation (Figure 4). This is exemplary of studies illustrating the influence of apoptotic recognition on tumor immunogenicity [89-90]. Characterization of these interactions, however, requires the use of specific cytometric markers, involving the use of cell-tracking and proliferation assays to assess the capacity of a given antigen or stimulus for immune activation. Carboxyfluorescein diacetate-succinimidyl ester (CFDA-SE) dye, for example, can be used to stain cells in a proliferation study. After diffusing into the cells, acetate moieties on the dye are cleaved, yielding the highly fluorescent dye CFSE. Because CFSE cannot permeate the cell membrane, it is retained in the cytoplasm through successive cell

divisions (halving the fluorescence intensity with each division). As a result, the proliferative capacity of a given cell type can be determined by assessing the fluorescence intensity of a given population of cells over time via flow cytometry. While studies of this type have allowed the study of complex immune signaling interactions, they remain complicated by the need for multiple stages of quantification and staining, each step of which increases the complexity of the system and the analysis of any changes that may take place. As such studies grow to include greater numbers of variables, it becomes increasingly difficult to conduct such complex experiments. In keeping with this trend, there is a general need for generalizable techniques capable of assessing immune activation and function. Furthermore, such techniques will enable researchers to compare results across experiments and across studies, allowing increased reach and significance for results achieved using this new generation of techniques.

## 1.4 Research Outline

The goal of this work is to extend the utility of the instrumentation developed by Block and colleagues to include label-free studies of cell attachment with single cell spatial resolution. This is first addressed through the investigation of a number of cellular processes with photonic crystal biosensors in conjunction with a modified fluorescence microscope. Processes investigated include cell growth, adhesion, differentiation, and programmed cell death. After verifying that these processes can be characterized using PC substrates, additional studies are performed to characterize

## 1.5 Figures

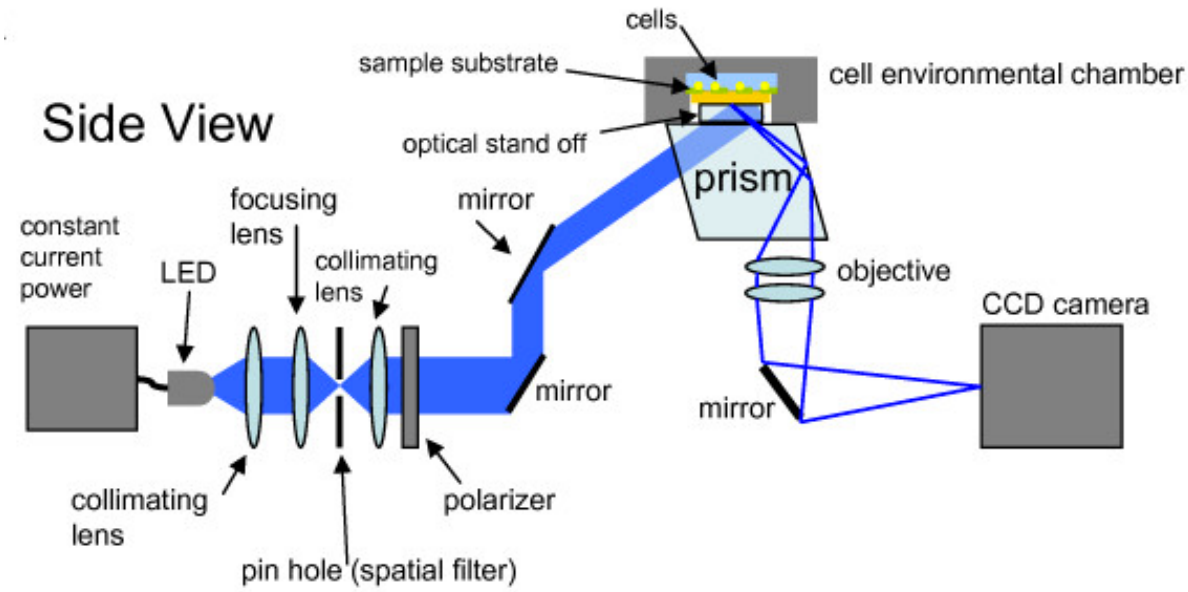


**Figure 1:** Schematic for SPR imaging instrument. Incident LED illumination is spatially filtered, collimated, and directed by mirrors through a SF-10 prism coupled to a commercially available cell environmental chamber designed for transmission and fluorescence microscopies. The reflected image is captured on a CCD camera [39].

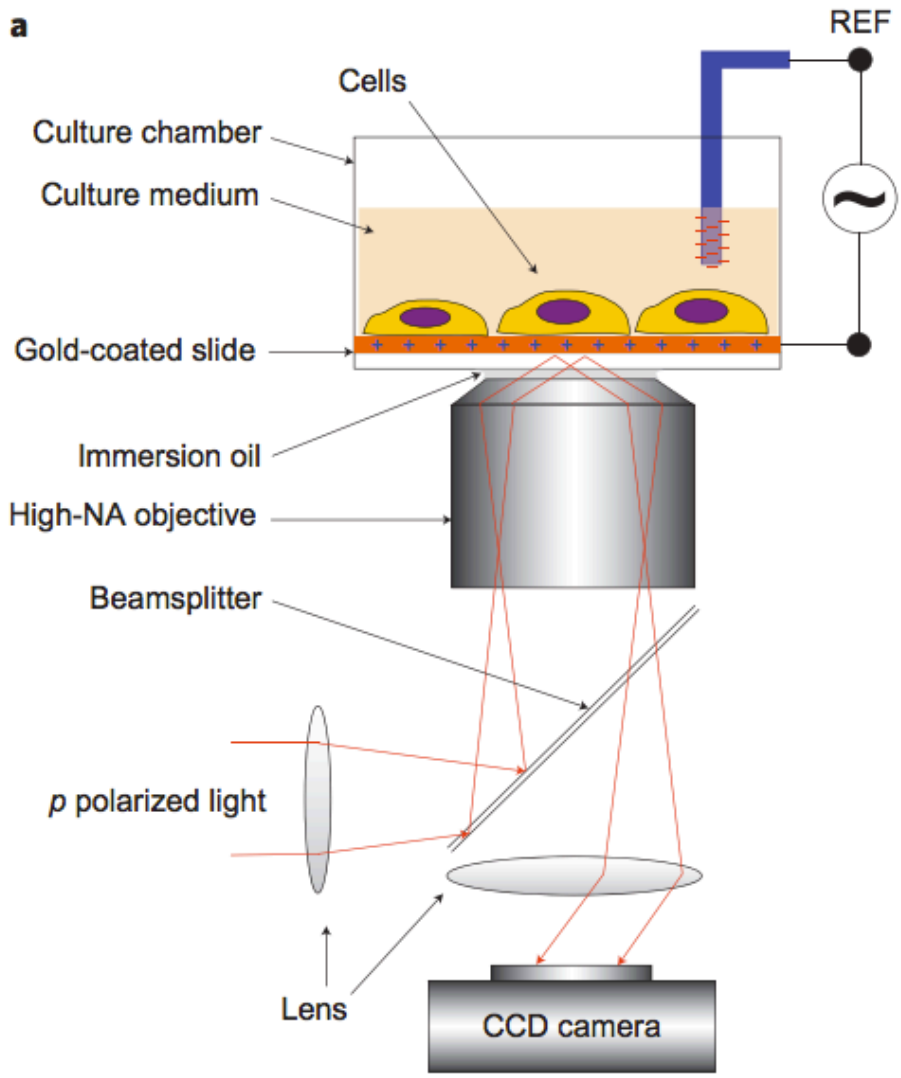


**Figure 2:** Schematic of Electrochemical Impedance Microscopy instrumentation. A laser beam (polarized light) is directed by lenses onto a gold-coated glass coverslip through an oil immersion high-NA (numeric aperture) objective to create SPR on the gold surface, which is imaged with a CCD camera. Cells are cultured for study on the gold-coated cover glass. An a.c. modulation potential is applied to the gold electrode relative to a reference electrode (REF) inserted in the culture medium solution. The EIM image is created from the potential-induced SPR signal changes. In addition to the SPR and EIM images, a conventional optical image of the same sample can also be recorded [Wang 2011].

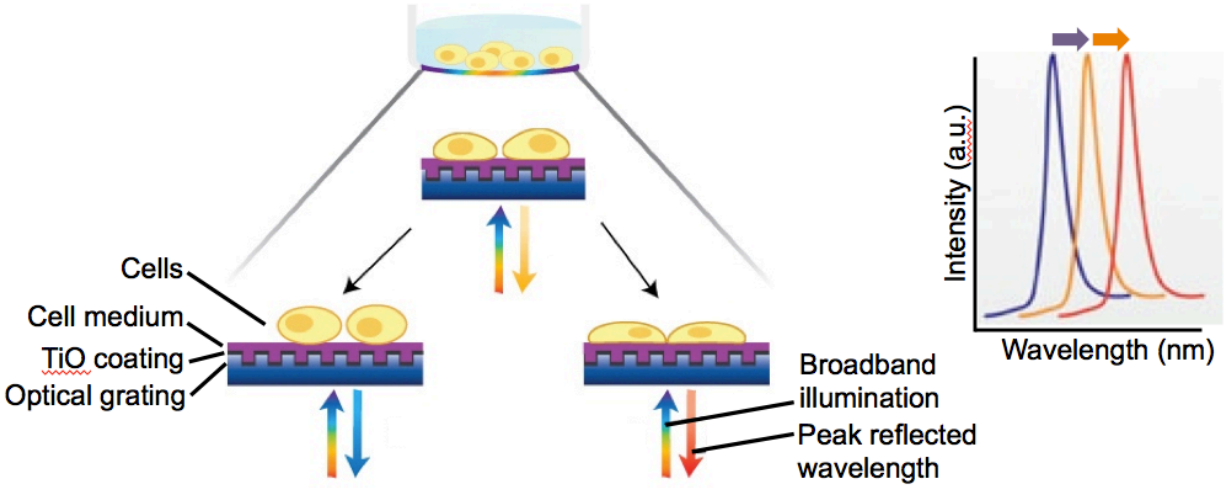


**Figure 3:** Schematic of a high-throughput photonic crystal biosensor configuration. Using an optical fiber, incident light from a broadband LED source is used to illuminate the PC biosensor from the bottom, at normal incidence. Another optical fiber is used to collect the reflected light, which is characterized by a spectrometer to assess the peak reflected wavelength (Peak Wavelength Value, PWV) for each biosensorl. As cells respond en masse to each other and varying extracellular conditions, their changes in attachment strength correspond with measured shifts in the PWV [Adopted from SRU Biosystems, Inc.].

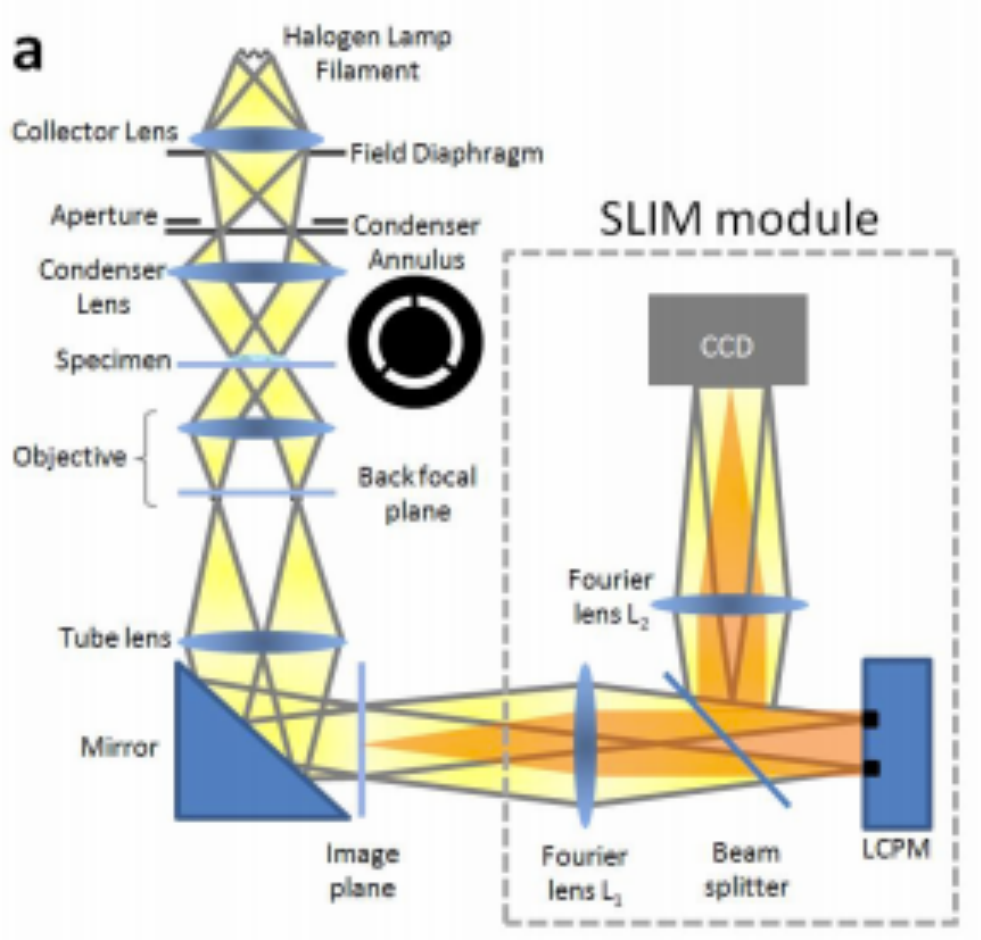


**Figure 4:** Fig. 1. Schematic setup for Spatial Light Interference Microscopy. The SLIM module is attached to a commercial phase contrast microscope (Axio Observer Z1, Zeiss, in this case). The lamp filament is projected onto the condenser annulus. The annulus is located at the focal plane of the condenser, which collimates the light towards the sample. For conventional phase contrast microscopy, the phase objective contains a phase ring, which delays the unscattered light by a quarter wavelength and also attenuates it by a factor of 5. The image is delivered via the tube lens to the image plane, where the SLIM module processes it further. The Fourier lens L1 relays the back focal plane of the objective onto the surface of the liquid crystal phase modulator (LCPM, Boulder Nonlinear). By displaying different masks on the LCPM, the phase delay between the scattered and unscattered components is modulated accurately. Fourier lens L2 reconstructs the final image at the CCD plane, which is conjugated with the image plane [Wang 2011].

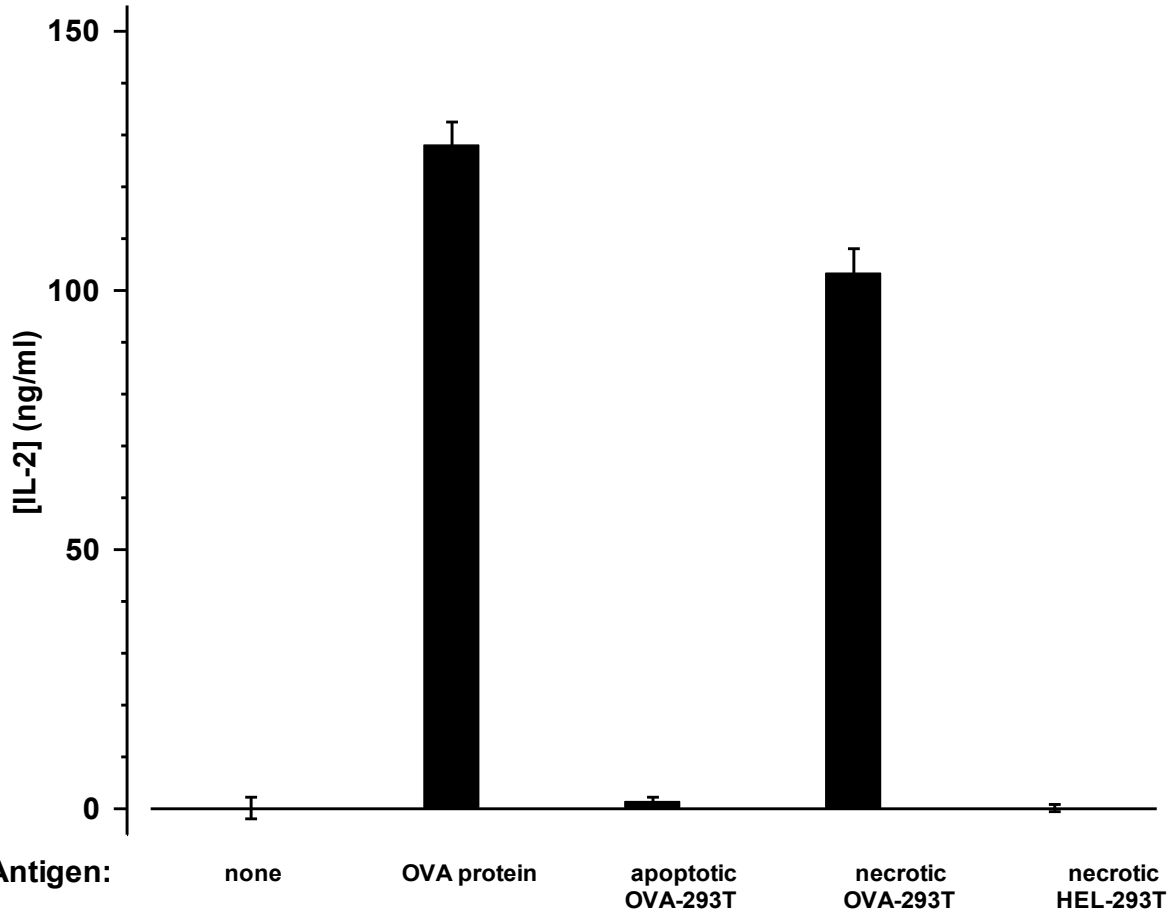


**Figure 5:** Antigen presentation by macrophages Is decreases markedly exposure to apoptotic cells. The presentation to DO11.10 T lymphocytes of antigenic chicken ovalbumin (OVA) peptide ($OVA_{323–339}$) by peritoneal macrophages was assessed as T cell-specific secretion of IL-2. Peritoneal macrophages were obtained from BALB/c mice (3 mo. of age). Macrophages were incubated without exogenous peptide, with whole ovalbumin protein, or with human 293T cells expressing ovalbumin that had been induced to undergo either apoptotic or necrotic death. As a control for antigenic specificity, macrophages were incubated with necrotic 293T cells expressing hen egg lysozyme (HEL-293T). LPS was added together with DO11.10 T cells, and the cultures were incubated for 18 hr. Secreted IL-2 from triplicate cultures was assessed by ELISA; results are expressed as the mean (± SEM) of these determinations. No IL-2 secretion was detectable in the absence of added T lymphocytes, and no stimulation of DO11.10 T cells by the human 293T cell targets occurred in the absence of macrophages. [Ucker et al., UIC]

# CHAPTER 2 – LABEL-FREE IMAGING OF CELL ATTACHMENT WITH PHOTONIC CRYSTAL ENHANCED MICROSCOPY

Cell adhesion is a vital process for cell growth, proliferation, differentiation and motility, playing a central role in such varied phenomena as tissue growth and development, inflammation, wound healing, cancer metastasis, and myriad others [4-5]. For life science research and cell-based pharmaceutical screening applications, development of a more fundamental understanding of the factors influencing cell-substrate interactions requires the development of new tools. Current *in vitro* cell imaging techniques often rely either on cytotoxic stains or fluorescent labels to provide highly specific information; both of these techniques frequently permanently alter the state of the cell, and often require fixing or isolation of the samples to be considered for examination. Traditional light microscopy and phase contrast microscopy offer improvements in the lengths of possible experimentation, but at the expense of specific and relevant information regarding cell activity and metabolism. In this chapter, photonic crystal enhanced microscopy (PCEM) is presented as a label-free imaging biosensor technique for visualizing and quantifying complex cellular responses to multiple stimuli over prolonged periods of study.

## 2.1 PC Biosensor Design

Photonic Crystal (PC) biosensors, also known as a type of guided mode resonant filter (GMRF), have been recently demonstrated as a high-resolution label-free detection technology that can be fabricated from plastic materials and incorporated into standard microplate formats for high throughput screening applications [41, 71]. PC biosensors consist of a low refractive index sub-wavelength periodic grating structure that functions as a highly reflective optical resonator (Figure 6). While previously reported photonic crystal surfaces have been comprised of a

rectangular grating profile with a period of 550 nm and a grating depth of approximately 150 nm, the biosensors used in this study have been modified to reduce possible effects of sensor morphology on the formation of cell attachments. To reduce the occurrence of such effects, the PC biosensors used in this study possess a period of 360 nm with a grating depth of approximately 30 nm. Additionally, the addition of an intermediary $SiO_2$ layer allows for the exposed $TiO_2$ layer of the sensor to be deposited with a gradual curved profile in lieu of the rectangular profile used in previously documented sensors. Atomic force microscopy imaging was performed to verify surface morphology would have a minimal effect on cellular activity (Figure 6). It is worth noting that none of the cells plated on these sensors did not exhibit any polarization with respect to the grating structure, though more mechanically sensitive cells may exhibit preferential orientation. When illuminated by a collimated laser, the PC surface acts as a highly efficient light reflector only at a specific angle of incidence at which resonant coupling of incident light to the PC occurs (Figure 7). The resonant coupling angle is dependent upon the dielectric permittivity of material on the PC surface, and shifts to lower angles when cells or biomolecules become attached. Because the PC surface effectively prevents lateral propagation of resonantly coupled light, attachment of discrete objects, such as cells, results in a highly localized shift in the resonant coupling angle, thus opening up the potential for high resolution biosensor imaging. This report presents a detection system based upon microscopy that overcomes spatial resolution limitations of previously reported PC biosensor imaging systems, [91-92] enabling, for the first time, label-free cell attachment images with 0.61 $\mu m^2$ pixel resolution. The detection system does not require physical contact to a coupling prism as required for imaging Surface Plasmon Resonance (SPR) [39, 93], nor the *a priori* knowledge of the analyte necessary for ellipsometry [94-95], therefore enabling high throughput measurement of large numbers of cells within biosensor-embedded microplates, flow channels, and culture dishes.

As described in Figure 8, the PCEM instrument illuminates the PC surface from below with a collimated laser beam, which is rapidly scanned through a ~3° range of incident angles at

0.01-degree increments with a computer-controlled rotating mirror. An image of transmitted light intensity is gathered through a 10x or 20x microscope objective onto a CCD camera for each incident angle (Figures 8-9). At the resonant coupling angle, the incident laser light is efficiently reflected, resulting in a minimum in transmitted intensity. Software determines the Angle of Minimum Transmission (AMT) on a pixel-by-pixel basis from the CCD images by fitting a second order polynomial function to the transmitted intensity versus angle curve (Fig. 6c). It is important to note that due to the limited penetration of the evanescent field region from the PC into the surrounding cell media (approximately 100 nm), PCEM is sensitive only to dynamic changes in biomaterial density at or near the cell surface, remaining unaffected by the presence and location of cellular organelles. As attachment, driven by the activity of integrins and filapodia, draws the cell into more intimate contact with the PC surface, there is a commensurate increase in the local dielectric permittivity that is clearly measurable (Figure 10). Detection resolution is sufficient not only for observation of large angle shifts that differentiate cell from non-cell regions, but also for observation of subtle changes in attachment strength that result from motility, apoptosis, differentiation, and contraction.

## 2.2 Materials and Methods

*Instrument Description*

The detection system used in our study is a modified back-illuminated fluorescent microscope (Olympus BX51WI) shown schematically in Figure 8. The microscope is equipped with 10x and 20x objective lenses (N.A. = 0.25, 0.40, respectively) and an electron multiplying CCD (C9100-13 EM-CCD; Hammamatsu Inc.) for imaging. A 300-mW, $\lambda$=637 nm AlGaInP diode laser is the excitation source. The laser light is passed through a rotating diffuser and then collimated by a beam expander. This sequence of optical components results in a spatially uniform, highly collimated beam that is then incident on a high-resolution motorized gimbal-mounted mirror, thus providing collimated illumination at a user-selectable incident angle. In order to maintain a constant

illumination area on the device, the gimbal-mounted mirror sits on top of a motorized linear stage that translates laterally as the mirror rotates. As the collimated light at a fixed wavelength is incident on the PC surface, the angle of incidence can be tuned to allow the laser to couple with the PC resonance, thereby allowing maximum field coupling into the transverse electric (TE) mode of the PC. The excitation illumination was TE polarized by passing the laser light through a half-wave plate.

*Device Fabrication*

Fabrication of the device was performed using a plastic-based nanoreplica molding process [71]. Briefly, a silicon wafer with a negative surface volume image of the desired grating pattern was fabricated using deep-UV lithography and reactive ion etching. A liquid that contains an uncured monomer and a UV-activated polymerization initiator is sandwiched between a flexible plastic sheet and the silicon master wafer to enable the liquid to fill the silicon surface structure subsequent to curing with a high intensity UV lamp (Xenon, Inc). The hardened polymer grating preferentially adheres to the plastic substrate, and thus can be easily peeled away from the silicon. After the molding step, the replica was cut and attached to a 1 × 3 $in^2$ microscope slide. An evaporated $SiO_2$ intermediate layer, ($t_{SiO2}$)= 200 nm, (e-beam evaporation, Denton Inc.) was deposited on the grating surface to control the resonant peak width. After the $SiO_2$ deposition, ~60 nm of $TiO_2$ was deposited by RF sputtering (PVD 75, Kurt Lesker) using an *in-situ* process monitor to accurately achieve a resonance condition that nominally results in $\lambda$=637 nm wavelength resonantly coupling to the PC surface at an incident angle of 4° in an aqueous environment. The device is bonded to a six well bottomless microplate using a transparent UV-curable adhesive (AC R260-A1, Addison Clear Wave). The plates were thoroughly rinsed and the wells were incubated with 70% ethanol for 15 min.

For Panc-1 and HepG2/C3 cell culture, the PC biosensors were coated with poly-*d*-lysine (MW = 70,000-150,000 Da, Sigma-Aldrich P6407) immediately prior to plating cells. For this

purpose the wells were incubated with a 100 ng/ml solution in cell grade phosphate buffered saline (PBS), pH = 7.4 for 15 min. After incubation, the wells were rinsed twice with PBS before cell media was added. For cardiomyocyte culture, bare sensor wells remained uncoated while fibronectin- and collagen-coated wells were rinsed with PBS before the addition of 2.0 ml of a solution containing 5.0 μg/ml fibronectin (Sigma-Aldrich F0895) and 20.0 μg/ml collagen (Sigma-Aldrich C8919) diluted in PBS. Wells were then incubated for 1 h at 37°C before rinsing three times with PBS. For adipose-derived stem cell culture, wells were rinsed with PBS prior to 1 h incubation with 2.0 mL 25 μg/mL collagen (Sigma Aldrich C8919) dissolved in 0.1M acetic acid in ultrapure water at 37°C. Wells were then rinsed three times with PBS immediately prior to cell culture.

*Materials and Cell Culture*

Cell culture media was obtained from the Cell Media Facility at the University of Illinois at Urbana-Champaign. Panc-1 cells, porcine adipose-derived stem cells, and neonatal rat cardiomyocytes were cultured in Dulbecco's modified Eagle's medium (DMEM) with 10% fetal bovine serum (FBS), 4 mM L-glutamine and penicillin-streptomycin. The HepG2/C3 cells were grown in minimum essential medium (MEM) with 10% FBS. PBS (pH 7.4) and poly-d-lysine (mol wt 70-150,000) were purchased from Sigma-Aldrich and trypsin (0.25% + EDTA) from Thermo scientific. Staurosporine was purchased from Sigma-Aldrich and dissolved in DMSO leading at a concentration of 1mg/ml.

All cell lines were grown in an incubator at 37°C and 5% $CO_2$ until 80% confluence and then passed using trypsin every 2-5 days as necessary. For imaging the cells were centrifuged to remove the trypsin and then resuspended in media and plated on the device in a total volume of 2 ml at a density of 4-6 x $10^4$ cells/mL. Cell counting was performed with a hemacytometer (Reichert).

*Cardiomyocyte isolation and culture*

Cardiomyocytes were obtained from 6-day old neonatal Sprague-Dawley rats (Harlan Laboratories, Inc.) using an approved protocol by the University of Illinois at Urbana-Champaign Institutional Animal Care and Use Committee (IACUC; Protocol #08190, Adopted from Maass et al., [12]). Briefly, whole hearts were excised from the rats and placed in 4°C HBSS buffer. Using small scissors, the left and right atria were removed and the remaining ventricles were quartered. The quartered ventricles were digested in 0.05% (w/v) purified trypsin (Worthington Biochemicals Corp.), while rotating gently at 4°C overnight. After 16 hours, warm growth medium was added for 5 minutes at 37°C to inhibit trypsin digestion. After washing and discarding the supernatant, 0.1% (w/v) purified type II collagenase (Worthington Biochemicals Corp.) was added for 45 minutes while rotating at 37°C. The tissue was gently triturated to mechanically loosen the cells, and the suspension was filtered through a 40-μm cell strainer. The suspension was removed after centrifugation at 150 x g for 6 min. The remaining cell pellet was re-suspended in warm growth medium and pre-plated for 1 hour to enrich for cardiomyocytes. The suspension was collected, and cardiomyocytes were seeded on polystyrene dishes. The growth medium consisted of high glucose (4.5 g/L) DMEM with 10% FBS. The cells were cultured in an incubator with 5% $CO_2$ at 37°C.

*Porcine adipose-derived stem cell isolation*

Adipose-derived stem cells were isolated from back fat of pigs that were 3 months of age, in compliance with University of Illinois IACUC approved procedures. Pigs were euthanized by an overdose of pentobarbital and fat samples were excised from the back proximal to the spine. Adipose tissues were cleaned and submerged in PBS (without Ca or Mg) containing 3X Penicillin/Streptomycin prior to being cut into 1-2mm width strips. The strips were then minced and incubated on a shaker in 2.5 mg/ml solution of collagenase (Sigma, C2674) in PBS at 37°C for 2-3 hours. The resulting solution was diluted 1:3 in PBS before centrifugation at 250 x g for 10 min.

Floating adipocytes were removed and the remaining PBS aspirated from the cell pellet followed by resuspension and washing 2x in PBS. Red blood cells were removed by the addition of red blood cell lysis buffer (Sigma, R7757) for 2-3 minutes. Cells were then diluted with 30 ml PBS and centrifuged at 120 x g for 5 min, followed by aspiration of the supernatant and resuspension in 48 ml Dulbecco's modified eagle's medium (DMEM) with 10% fetal bovine serum. The resulting suspension was filtered twice through sterile gauze before additional centrifugation at 120 x g for 5 min and resuspension in 20 ml DMEM with 10% FBS. The cells were then filtered through a 100 μm nylon cell strainer (Fisher, 22363549), prior to counting with a hemacytometer (Reichert). Cells were then plated at 5-10 x $10^3$ cells per $cm^2$ in low glucose (1.0 g/L) DMEM with 10% fetal bovine serum prior to incubation in a low (5%) $O_2$ incubator. Cells were cultured for 48 h prior to the first media change, and passaged at confluency. Cell aliquots were frozen at less than passage 5.

*Porcine adipose-derived stem cell culture and differentiation*

Thawed ADSCs were cultured in low-glucose (1.0 g/L) DMEM with 10% FBS, penicillin-streptomycin, 2.9 g/L L-glutamine, and 0.2 g/L HEPES. Cells were cultured in an incubator maintained at 5% $CO_2$, 37°C. ADSCs were passaged no more than 5 times. For PCEM imaging, ADSCs were washed with PBS (without Ca2+, Mg2+), trypsinized using 0.25% trypsin (CellGro), and plated on PC biosensors in 2.0 ml at a density of 5.0 x $10^4$ cells/ml. To induce ADSC differentiation and development of dendrite-like cell projections, treated cells were exposed to a neurogenic induction medium containing 200 nM butylated hydroxyanisole (BHA), 2 mM valproic acid, 10 mM forskolin, 5mg/ml insulin, 2.5 mM KCl, and 25 mM hydrocortizone in solution with high-glucose (4.5 g/L) DMEM [99].

*Statistical Analysis*

Two-tailed student's *t* tests were performed for the results described in Fig. 7-8 with $p < 0.05$ used to signify statistical significance. All *p* value determinations were two-tailed. GraphPad

software (LaJolla, CA) was used for all calculations concerning statistical evaluation. Error bars indicate one standard deviation from the mean.

## 2.3 Results

*Dynamic Label-Free Imaging of Cell Attachment*

The imaging procedure is described in Figure 6 using HepG2/C3 hepatic carcinoma cells. Selected images are cropped and enlarged to show detail; cells were cultured on large (~1.75cm$^2$) sensor areas, and several 400 μm x 400 μm images were taken for each timepoint. To demonstrate the abilities of this label-free assay to detect cell attachment at a single-cell level, these images were cropped to the size of a few exemplary cells for the creation of each figure. The image shown in Figure 6a was recorded at an angle below both cell and background resonance conditions, and provides morphological information similar to traditional bright field microscopy. Red and blue circles in Fig. 6a mark the locations of pixels for which transmission intensity is plotted as a function of angle of incidence in Figure 6b. In Figure 6c, the final PCEM image displays AMT for each pixel as a function of position presented as a false-color composite. Cell attachment shifts the local resonance to a lower value as indicated by the red color. The bright field image, used in tandem with the PCEM image, can be used to correlate structural and morphological information with the cell attachment spatial distribution (Fig. 6d).

Comparison of the brightfield image with the PCEM image shows an increased footprint area in the PCEM image; this is attributed to a combination of the formation of lamellipodia and the presence of a spreading effect due to finite propagation lengths of the sensors. In a previous study, similarly configured photonic crystal biosensors demonstrated a detection resolution of 3.5 um in the direction parallel to the grating lines, and diffraction-limited resolution in the direction perpendicular to the grating lines [96]. These sensors described were used to generate AMT shift images, for which a slight smearing effect was observed. For DNA microarray spots generating an AMT shift of 0.38º, this effect could be observed within 8 um in the direction parallel to the grating, and within 1 um in the direction perpendicular to the grating [74]. The most significant effect of this limitation for this study is a spreading effect seen at boundaries, which is slightly more pronounced

in the direction of the grating due to the orientation dependence described above. As the AMT shifts typically exhibited by cells are on the order of 0.1 – 0.2º, the cell attachment footprints measured by PCEM accurately reflect the cell boundaries within an uncertainty of ~4 um in the direction parallel to the grating, and within ~1 um in the direction perpendicular to the grating.

PCEM imaging is currently performed in a transmissive setup through a microscope slide and cell media, so it is likely that spatial resolution can be improved with the construction of a reflection-based detection instrument to avoid potential issues arising from sample-induced diffraction and absorption. Scans completed in this study ranged from 1.5º - 2.0º at 0.01º increments. As each image takes approximately 50 ms to collect, it takes approximately 30 s to collect and save the images required to build a PCEM image for one frame. The computation required to compose the final image requires an additional ~15 s, allowing a final temporal resolution of approximately one frame per minute. As a result, cellular processes taking place on faster time scales may elude the PCEM processing modality in its current state, though scanning over a smaller range of angles or delaying image processing until conclusion of the study would result in moderate increases in sampling rate.

To demonstrate long-term application of PCEM, HepG2/C3 cells were plated on a poly-*d*-lysine (PDL)-coated sensor and the progress of their attachment was imaged via PCEM after 1, 2, 4 and 23 hours in culture. After one hour in culture, the HepG2/C3 cells show evidence of cell attachment, presenting average AMT shifts of 0.25 ±0.01° (1 S.D.) from background resonance. Throughout the time course, multiple changes in cell morphology can be seen in the bright field images, including changes in cell shape, size, and orientation throughout the experiment (Fig. 7). The PCEM images follow the changes in cell morphology observed in the bright field images, tracking the movement of the cell across the top of the field. Importantly, cells that translocate and cells that detach completely leave little to no evidence in the way of a footprint (Fig. 7, open arrows); this serves as further confirmation that the increased mass density causing AMT shift is caused by the presence of proteinaceous cell attachments, and not merely material adsorption

from culture media or cellular secretion. Similarly, as cells spread and create more pronounced attachments, areas of new attachment as indicated via brightfield microscopy show increased AMT shift via PCEM (closed arrows, Fig. 7). The relationship between PCEM images and bright field images lends PCEM extensive utility in tracking the relationship between dynamic cell activity and attachment footprint. At the 23-hour time point, PCEM images reveal that the cell areas interacting with the substrate are substantially larger than what may be inferred from bright field examination alone. Furthermore, the lateral resolution is sufficient to analyze variability of attachment within a single cell. The dark red color in the cell centers seen in the PCEM images indicates that attachment density is greatest at these locations.

*Correlation with ECM-Dependent Physiologic Changes*

To demonstrate the ability of PCEM to resolve cellular changes in response to external stimuli, apoptosis was induced in Panc-1 human pancreatic cancer cells. Panc-1 cells were cultured on the sensor surface coated with PDL for 24 hours before treatment with 10 ug/ml staurosporine (Figure 8). The morphological changes caused by staurosporine treatment are evident in the reduced definition of the cell border and rounded morphology shown in the bright field images. To characterize the cell response using PCEM, individual pixels were chosen from regions on the cell body (blue), on the cell periphery (green), and on the background (red). The selected regions are marked with circles on a bright field image and the curves for each pixel are given in the corresponding color in Figure 8a. Prior to treatment, the curves for both pixels on the cell body and the cell periphery overlap and display an AMT shift of 0.10° from background. After treatment, the pixel residing on the cell periphery presents a curve more closely resembling that of the background, indicating decreased protein density at this location. The cell body remains on the surface, but causes a smaller AMT shift from background, indicating a weakening of attachment. Finally, PCEM images display the decrease in attachment across the cell, as indicated by a lower AMT shift from background. This provides confirmation that cell attachment does not permanently alter the sensor surface but rather presents a transient increase in dielectric permittivity for the duration of cell attachment at that location on the biosensor.

Another interesting application of PCEM is concurrent monitoring of cell physiology, morphology, and attachment density. Cardiomyocytes require fibronectin-dependent integrin-mediated cell attachments for optimal development and contractility [74]. To verify that PCEM is capable of detecting significant differences in cell attachment caused by changes in the available ECM substrate, primary neonatal rat cardiomyocytes were isolated and cultured on an uncoated PC biosensor and on a biosensor coated with a combination of collagen and fibronectin [97]. At 24 hours the cells were imaged via PCEM, and their morphologies and beating rates were recorded (see Table 1). Cells cultured in the absence of fibronectin showed greater frequency of rounded

morphology, and showed a complete lack of contractility (Fig. 9a, 9b). Cells cultured in the context of both fibronectin and collagen, however, showed a significantly greater frequency of stretched morphology, and exhibited an increased proportion of contractile cells (Fig. 9b). Additionally, contractility was exhibited only among cells showing a stretched morphology, supporting the fact that fibronectin-dependent cell attachment is critical for cardiac myocyte growth and differentiation are dependent on. AMT shift was evaluated over 70- to 100- pixel regions on and off each cell, enabling local background comparisons to be performed for each cell (see Supplementary Table 1 online). PCEM results confirmed the morphological observations, as cardiomyocytes exhibiting stretched morphology showed the greatest amount of AMT shift from background, and significantly greater amounts of AMT shift in comparison to their rounded counterparts, independent of the coating applied to the sensor surface (Fig. 9b, $p = 0.0133$ and $p < 0.0001$ for coated and uncoated sensors, respectively).

*Characterization of Stem Cell Differentiation*

To demonstrate the capacity of PCEM for label-free assessment of cell differentiation, porcine adipose-derived stem cells were exposed to a neurogenic induction medium, and PCEM was performed before and after administration. The induced morphological changes are typical of neurogenic differentiation, characterized by retraction of the cell body and the development of small, dendrite-like cellular projections [7, 98] (Fig. 9c). These changes were accompanied by a significant reduction in cell attachment as determined by a decrease in AMT shift (Fig. 9d, $p = 0.0007$). As the neurogenic induction protocol stimulates remodeling of the cytoskeleton and cell attachments, decreased attachment protein density is to be expected. The agreement of PCEM with this assertion demonstrates that the technique can be used to characterize the progression of stem cell differentiation without disturbing the process with fluorescent labels or cytotoxic endpoint assays.

This work demonstrates several new capabilities of PC biosensors using PCEM. The technique is capable of visualizing dynamic cell attachment with a pixel resolution of less than one micron, enabling highly detailed quantification of attachment distribution within individual cells. The label-free aspect of PCEM enables the prolonged study of cell-ECM attachment evolution in the context of cell growth, locomotion, differentiation, and apoptosis. The ability to functionalize PC biosensors with multiple cell-amenable coatings allows the study of the effects of substrate composition on cell attachment. PCEM also allows direct comparison between bright field and PCEM images, enabling correlation of cellular morphology with changes in attachment density. This combination of capabilities provides a unique new tool for study of cell attachment in many contexts, including wound healing, cell culture optimization, stem cell differentiation, and cancer metastasis.

## 2.4 Discussion

The importance and utility of label-free imaging have recently been underscored by an expansion in the number of techniques to acquire such data as well as by a growing need for improved understanding for a number of cellular processes. The use of fluorescent and chemical labels remains invaluable for the study of specific proteins and biochemical interactions, but the specificity such techniques provide often comes at the cost of decreased cell viability and a limited ability to study the same cells over extended periods of time. Such techniques also necessitate the use of one or several exogenous chemical markers in the area of interest within the cell, which introduces the possibility of obscuring the phenomenon of interest as it occurs in the absence of such labels. With the emergence of label-free techniques including surface plasmon resonance imaging (SPRi), ellipsometric microscopy, it has become possible to gain information complementary to that provided by traditional light microscopy. By decreasing the complexity of the experimental system, these techniques are in fact capable of investigating model systems with greater fidelity to their *in vivo* counterparts.

Despite this advantage, label-free imaging technologies continue to work against several challenges. While SPRi has enjoyed the ease of implementation associated with traditional surface plasmon resonance scanning techniques, one persistent area of difficulty is brought about by the lateral propagation of surface plasmons, which occurs on the order of several tens of microns [100]. This restricts the spatial resolution achievable with SPRi to distances on the order of entire cells, limiting the possibilities for its use in subcellular imaging. Similarly, ellipsometric imaging techniques have met with moderate success due to the comparatively small refractive index differences present in biological samples surrounded by aqueous media. PC biosensors seem to make several of these problems more tractable – it is possible to construct PC-based sensors with propagation lengths of less than 5 microns, and sensors generally exhibit high sensitivity with

regard to biological samples including proteins, nucleic acids, and whole cells immersed in aqueous media [4].

As the PCEM instrumentation registers shifts in transmitted wavelengths rather than changes in intensity, PCEM remains insensitive to the detection of particles passing transiently through the field of view. This represents another advantage over intensity-based detection assays, which may demonstrate susceptibility to artifacts in the presence of soluble particles capable of absorbing wavelengths of interest for analysis. Materials that adsorb to the sensor surface that also strongly absorb light at the laser wavelength have been documented to extinguish the PC resonance. In such a case, the resonance disappears, and the AMT fitting algorithm no longer functions [38]. Such regions are automatically recognized by the instrument software. Although no such cases were observed for the experiments conducted in this work, this technique has been used to measure deposition of light-absorbing hydroxyapatite produced by surface-attached stem cells that have differentiated to become osteoblasts.

In this work, PCEM was demonstrated as a useful tool to study a number of biologically interesting questions regarding cell attachment in several contexts. Because this new technique grants access to previously unavailable information, it will allow the achievement of a greater level of understanding not only in fundamentally interesting areas of cell biology, but also clinically relevant questions such as what types of cellular changes enable cancer metastasis, and what kinds of biomaterials and biocompatible polymers might best be applied to increase wound healing and recovery in the absence of inflammation and scarring. Questions such as these will require an unprecedented understanding of the extracellular matrix as well as of the cells interacting with that ECM. In future work, PCEM may be used in combination with existing technology to increase our understanding of the biology underlying problems like cancer metastasis, wound healing, axonal repair, and ischemic damage. The combination of PCEM with specific fluorescence labeling, for example, will allow the investigation of individual protein and signaling interactions in such contexts with respect to their influence on cell attachment. Modeling disease systems and using recently

developed biomaterials on PC biosensors with this new technique will allow new insight into these problems, enabling researchers to develop more successful therapeutic approaches to clinical disease.

## 2.5 Figures and Table

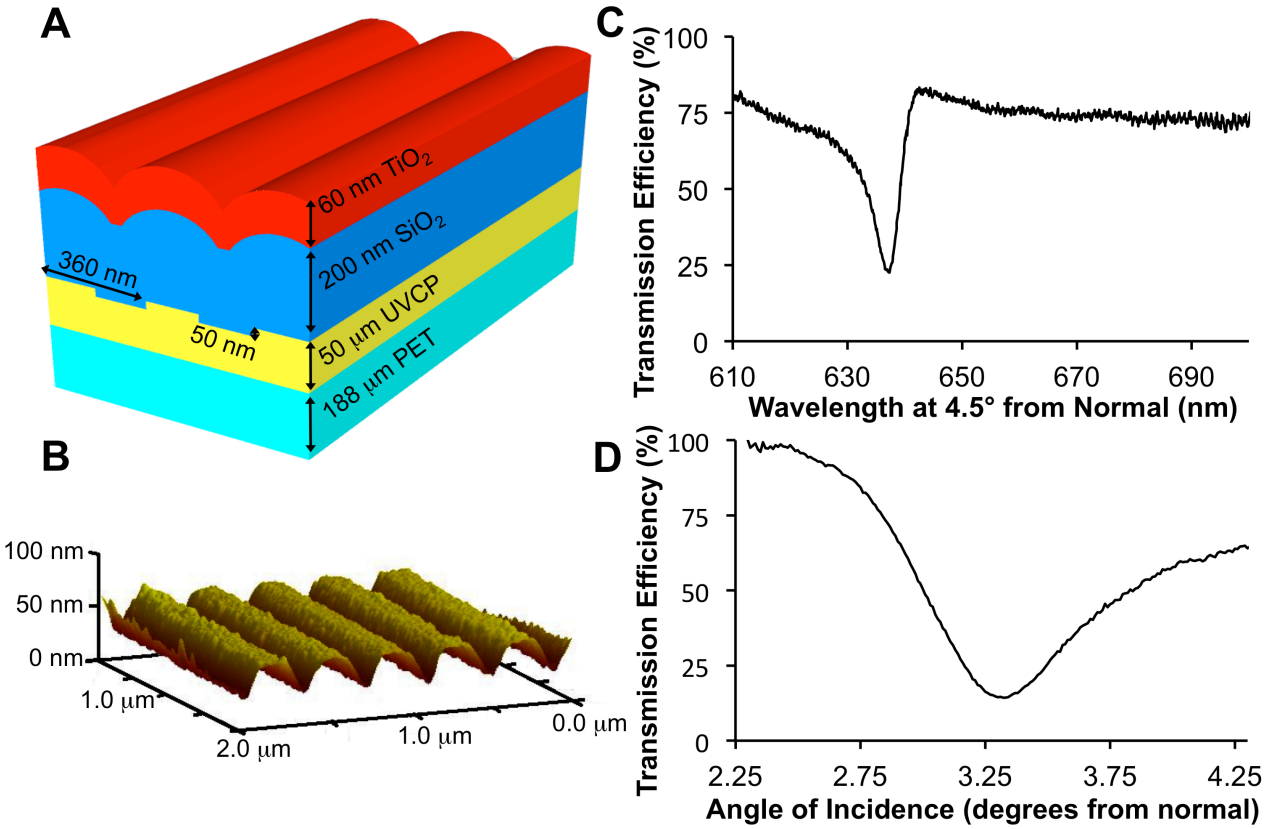


**Figure 6:** a) Schematic illustration of the PC biosensor configuration. A photoreplica molding process yields a grating pattern composed of UV-curable polymer (UVCP), which is affixed to a layer of polyethylene terephthalate (PET). The resulting grating is then coated with $SiO_2$ and $TiO_2$ to complete fabrication. b) PC biosensor characterization by wavelength. The resonant wavelength of a PC biosensor is rejected by the biosensor structure, resulting in decreased transmission efficiency. c) PC biosensor characterization by angle of incidence. The resonant angle of incidence in combination with the illumination using the resonant wavelength results in satisfaction of the resonant condition of the PC biosensor, resulting in decreased transmission efficiency.

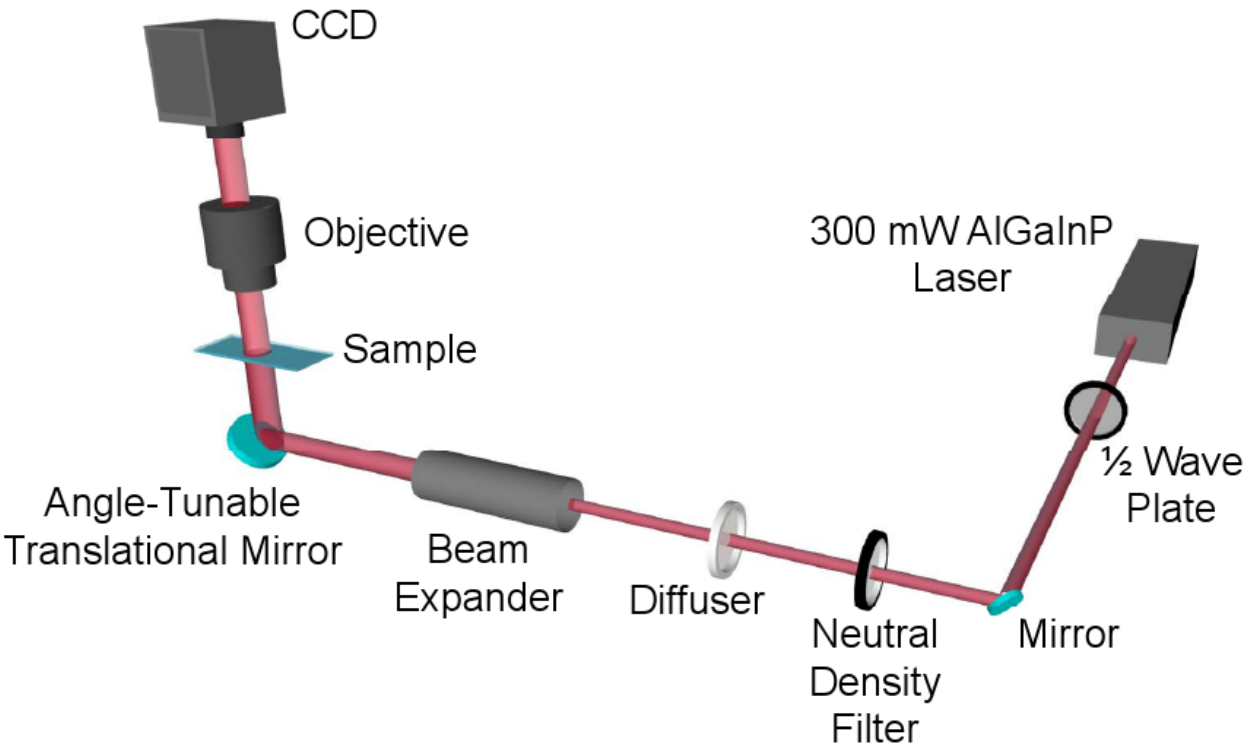


**Figure 7:** Schematic depiction of the photonic crystal enhanced microscope. Collimated 637 nm light emitted from a diode laser is directed into a ½ wave-plate for control of polarization before being attenuated by a variable neutral density filter. The beam is then directed through a diffuser and into a beam expander to provide a broadly uniform illumination source. The angle of incidence upon the sample is controlled by an angle-tunable mirror mounted on a translational stage. Transmitted light is magnified and focused by an objective lens and recorded by a CCD.

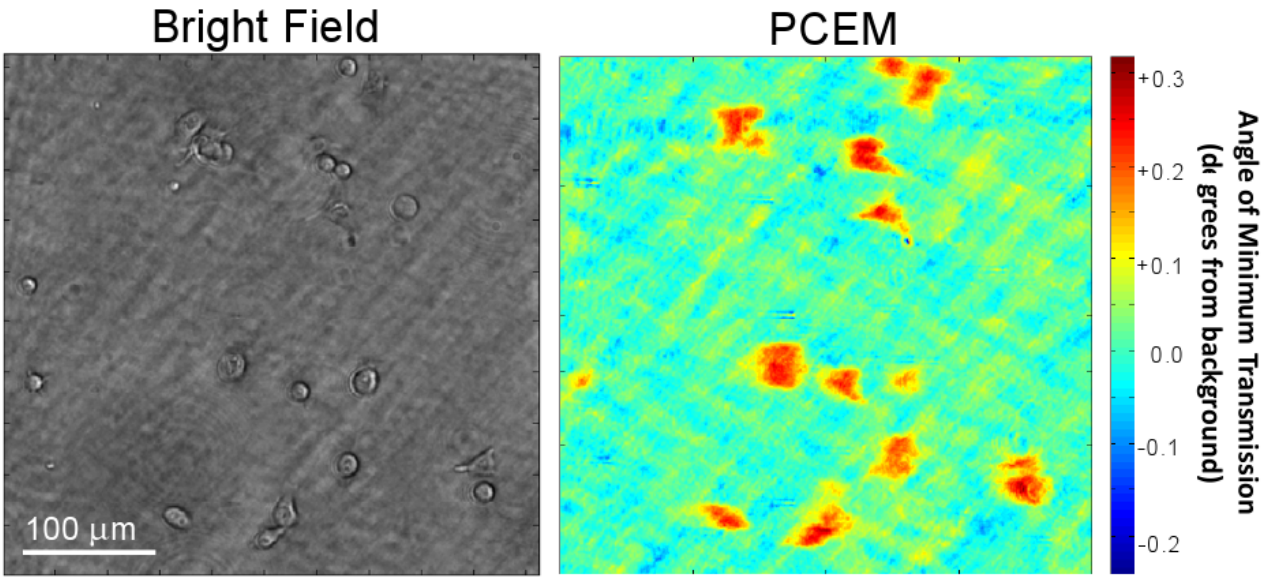


**Figure 8:** Wide-field capability of PCEM. PCEM imaging allows simultaneous label-free and bright field imaging of cell attachment over wide areas. At 20x magnification, the field of view encompasses an area of 0.16 $mm^2$.

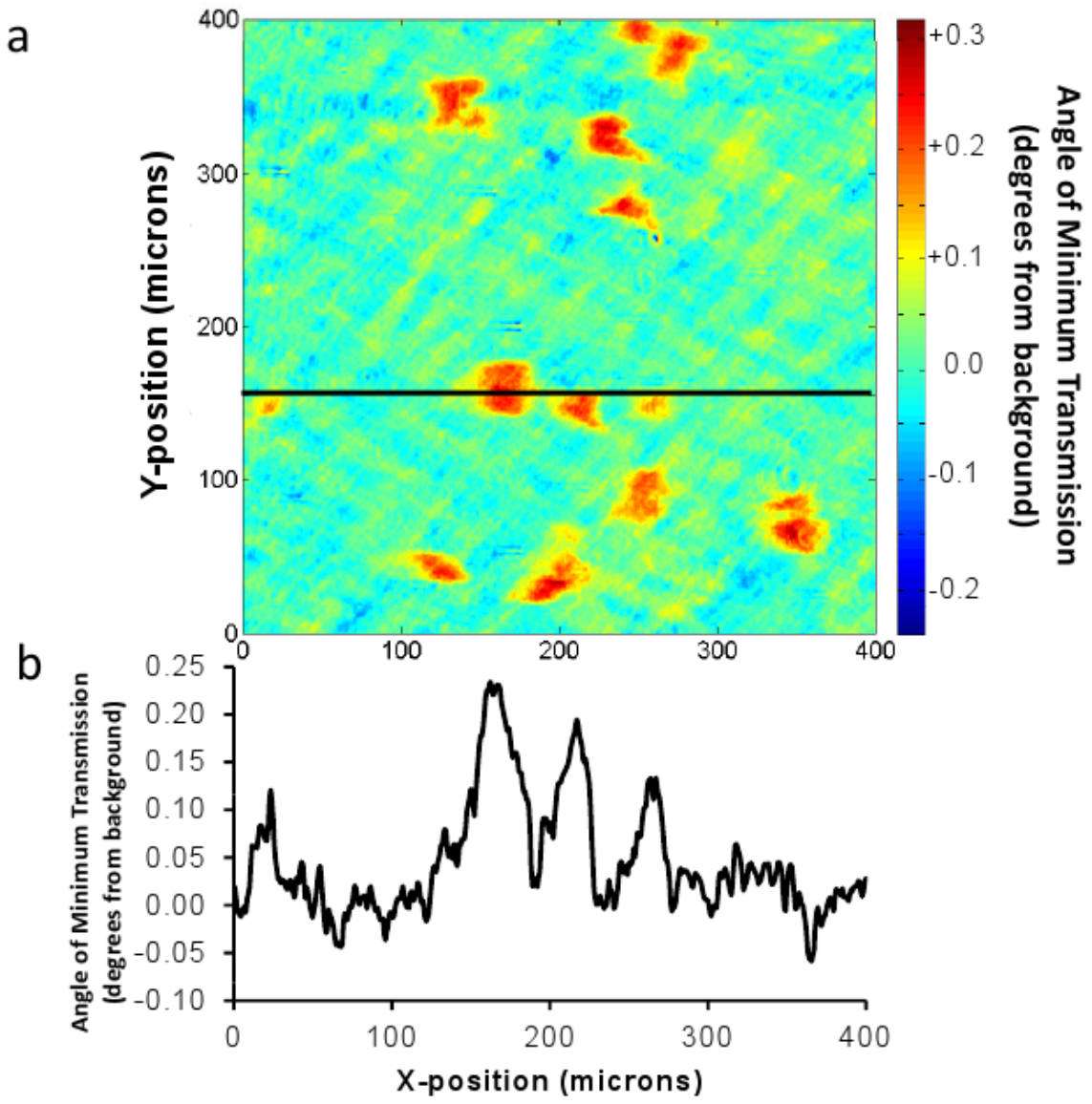


**Figure 9:** PCEM Line Plot. HepG2/C3 hepatic carcinoma cells cultured for 2h show significantly increased attachment protein density, as indicated by PCEM (a) and a line plot taken across the AMT profiles of three cells (b).

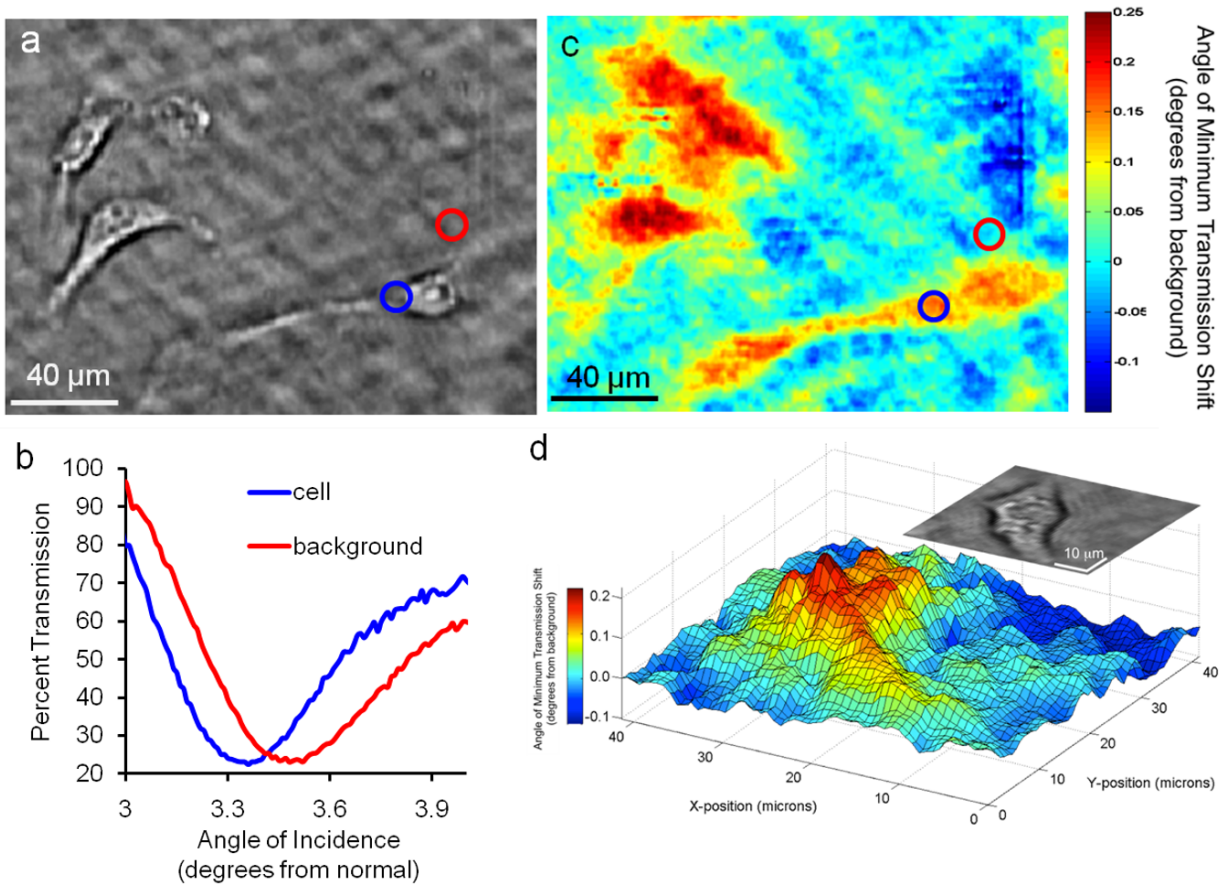


**Figure 10:** Summary of Photonic Crystal Enhanced Microscopy. a) Bright field microscopy of HepG2/C3 cells shows cell spreading and morphology. b) Transmission intensity is plotted as a function of angle of incidence for individual pixels on (blue) and off (red) a cell. Pixel regions are highlighted in (a). c) A composite PCEM image, describes the angle of minimum transmission (AMT) as a function of position. Attachment proteins deposited on the biosensor by viable cells result in a reduced angle of minimum transmission shift. d) A surface plot of cardiomyocyte attachment at 24h obtained via PCEM corresponds with the morphology observed in bright field microscopy (inset).

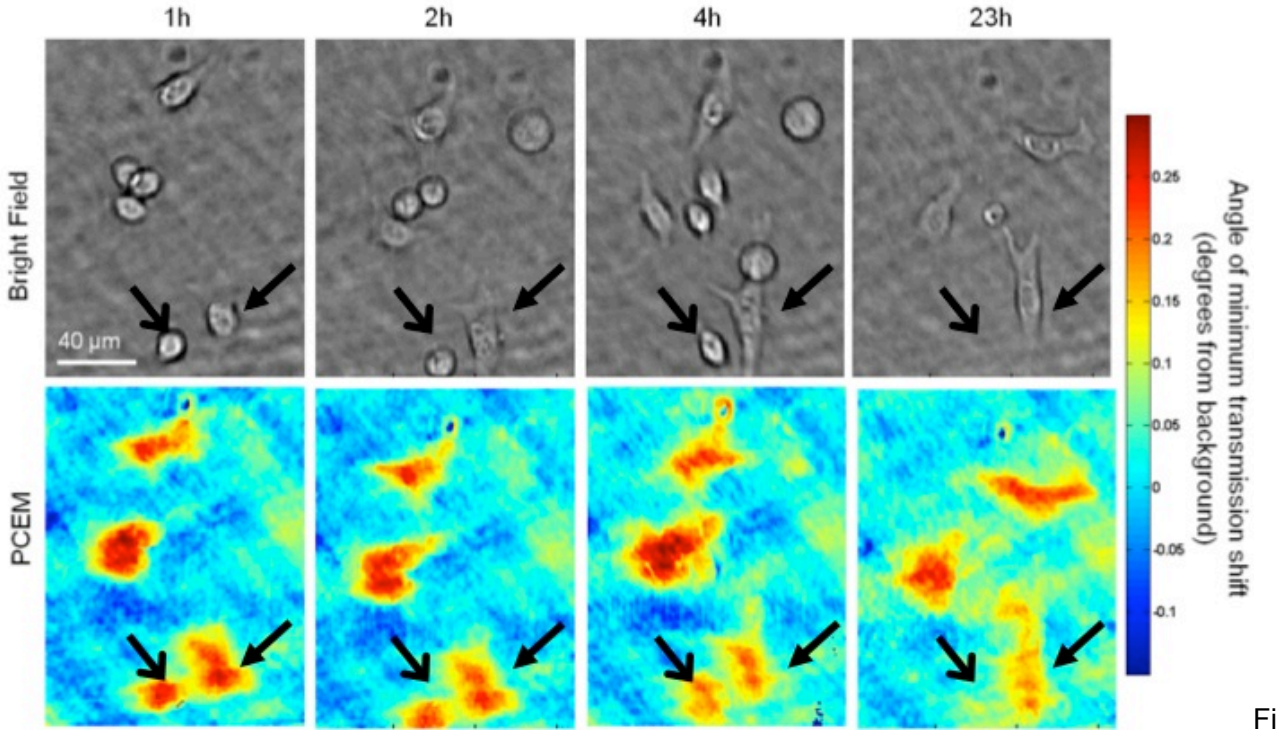


Fi

**Figure 11:** PCEM observation of cell growth and movement. HepG2/C3 hepatic carcinoma cell growth and locomotion were recorded over a 23-hour period via PCEM. The PCEM timecourse shows evidence of cell migration (closed arrow) as well as of cell detachment (open arrow).

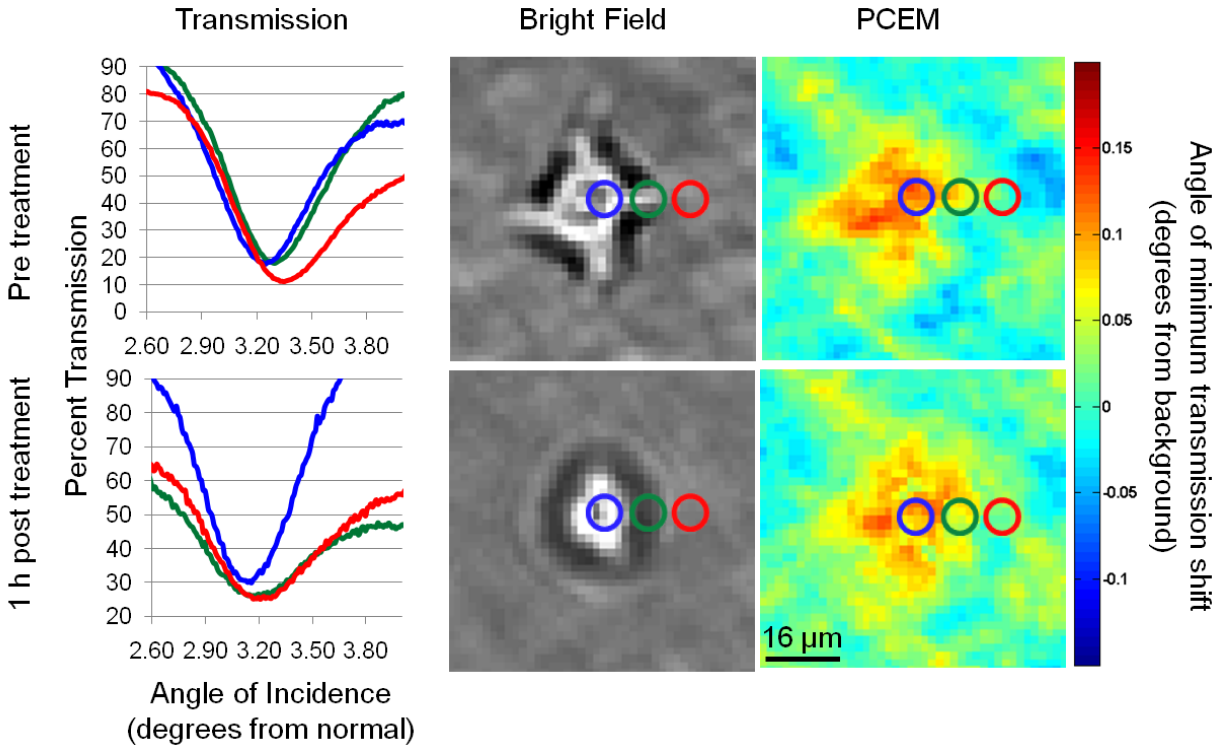


**Figure 12:** PCEM can be used to detect changes caused by apoptosis. Three individual pixels were chosen from regions on the cell body (blue), on the cell periphery (green), and outside the cell boundary (red). Intensity of transmission at is plotted as a function of angle of incidence. Curves generated for pixels on the cell body and the cell periphery overlap before treatment with staurosporine, indicating the presence of protein-dense cell attachments in these regions. PCEM shows decreased cell attachment after induction of apoptosis via staurosporine administration, and retraction of peripheral cell attachments (green) is supported by PCEM data.

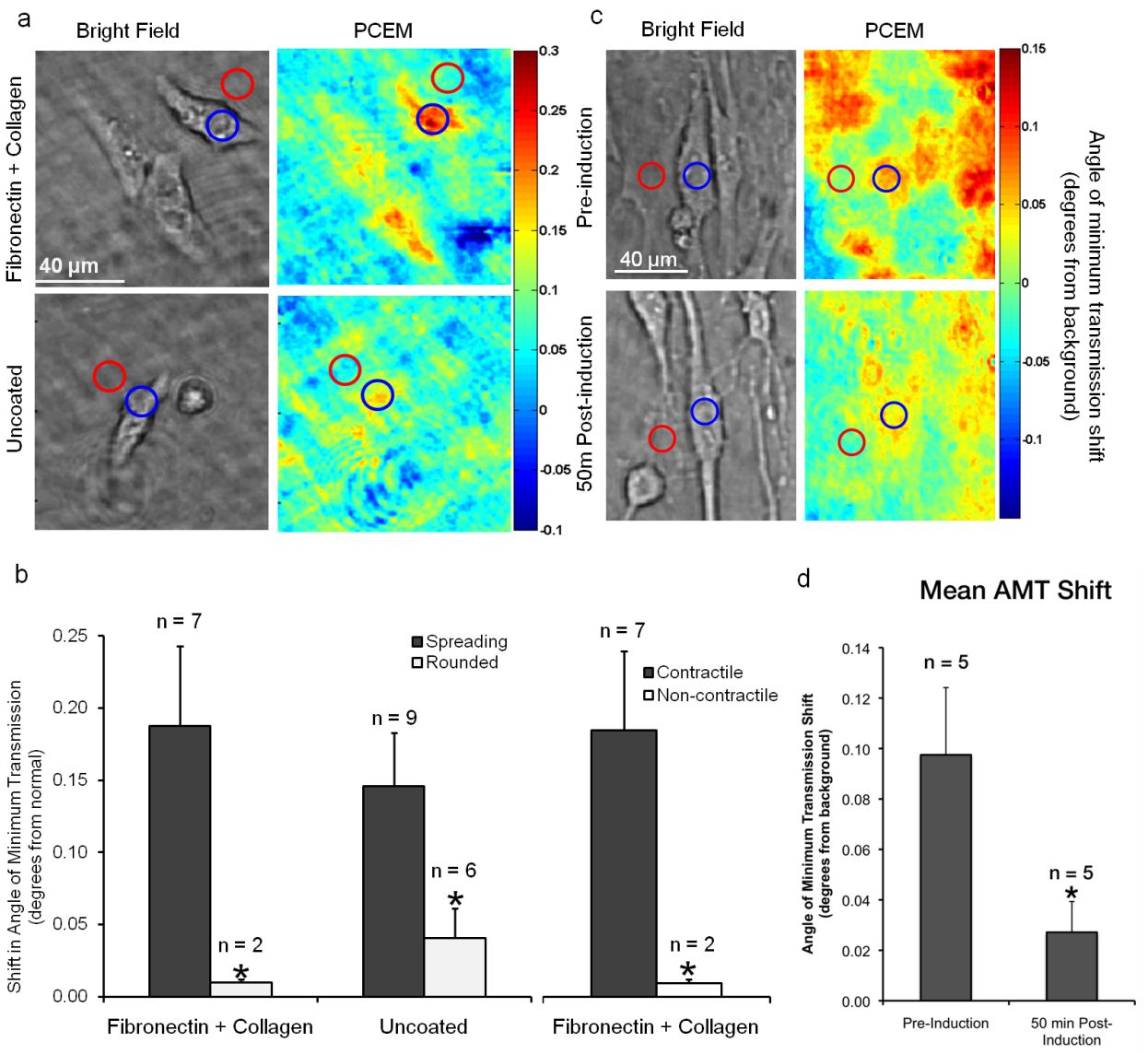


**Figure 13:** PCEM imaging of cellular responses brought about by extracellular stimuli. Blue circles indicate sample regions of interest used to measure AMT on individual cells, while red circles indicate sample regions of interest used to perform local background AMT measurements. a) Cropped bright field and corresponding PCEM images are shown for neonatal rat cardiomyocytes in culture on uncoated as well as fibronectin- and collagen-coated PC biosensors. b) On both coated (fibronectin + collagen) and uncoated sensors, cells exhibiting stretched morphology showed greater AMT shift then their rounded counterparts ($p$ = 0.0133 and $p$ < 0.0001, respectively). Contractile cells also exhibited significantly greater AMT shift than non-contractile cells cultured on coated sensors ($p$ = 0.0133). c) Forced differentiation of porcine adipose-derived stem cells with neurogenic induction medium stimulates the production of dendrite-like cell projections and retraction of cell bodies. d) Cells prior to treatment showed significantly greater attachment protein density than cells after treatment ($p$ = 0.0007).

Table 1: Data recorded for evaluation of cardiac myocytes in culture on PC biosensors coated with fibronectin and collagen, as well as for cardiac myocytes in culture on uncoated PC biosensors.

| Cell | ECM Coating | AMT Shift (degrees from background) | Standard Deviation | Contractility | Spreading |
|---|---|---|---|---|---|
| 1 | fibronectin, collagen | 0.181 | 0.026 | + | + |
| 2 | fibronectin, collagen | 0.168 | 0.011 | + | + |
| 3 | fibronectin, collagen | 0.215 | 0.037 | + | + |
| 4 | fibronectin, collagen | 0.224 | 0.024 | + | + |
| 5 | fibronectin, collagen | 0.276 | 0.023 | + | + |
| 6 | fibronectin, collagen | 0.134 | 0.011 | + | + |
| 7 | fibronectin, collagen | 0.008 | 0.014 | - | - |
| 8 | fibronectin, collagen | 0.011 | 0.024 | - | - |
| 9 | fibronectin, collagen | 0.113 | 0.026 | + | + |
| 10 | uncoated | 0.161 | 0.026 | - | + |
| 11 | uncoated | 0.181 | 0.131 | - | + |
| 12 | uncoated | 0.143 | 0.017 | - | + |
| 13 | uncoated | 0.01 | 0.024 | - | - |
| 14 | uncoated | 0.109 | 0.021 | - | + |
| 15 | uncoated | 0.02 | 0.011 | - | - |
| 16 | uncoated | 0.185 | 0.019 | - | + |
| 17 | uncoated | 0.096 | 0.018 | - | + |
| 18 | uncoated | 0.059 | 0.014 | - | - |
| 19 | uncoated | 0.033 | 0.033 | - | - |
| 20 | uncoated | 0.022 | 0.025 | - | - |
| 21 | uncoated | 0.04 | 0.018 | - | - |
| 22 | uncoated | 0.052 | 0.016 | - | - |
| 23 | uncoated | 0.071 | 0.009 | - | - |
| 24 | uncoated | 0.058 | 0.016 | - | - |

# CHAPTER 3: LABEL-FREE DETECTION OF CELL-CELL SIGNALING AND SPECIFIC APOPTOTIC RECOGNITION WITH PHOTONIC CRYSTAL BIOSENSORS

Apoptosis is a complex event essential for normal growth and development. With respect to tumor development, apoptotic signaling events exert significant influence inflammation, tumor immunogenicity, and disease state. Although the complex nature of these signaling interactions has presented challenges for their study and characterization, photonic crystal biosensors have been demonstrated to possess utility for a number of biological and biochemical screening applications. In this chapter, the first label-free quantitative detection of specific apoptotic recognition is described, using photonic crystal biosensors in a high-throughput screening (HTS)-capable microwell plate format. Furthermore, results are corroborated through the use of Photonic Crystal Enhanced Microscopy (PCEM), demonstrating apoptotic recognition and resulting activation at the cellular level. Notably, this work is the first documented detection of cell-cell signaling between disparate cell types using label-free techniques. Combining HTS and PCEM modes, it is possible for basic scientists to identify key determinants of immunogenicity and approaches for pharmacological control over their actions.

## 3.1 Apoptosis and Cell Attachment

Apoptosis is the primary mechanism of physiologic cell death, and is required for normal growth, development, and homeostasis. Apoptotic cells display many intracellular components as autoantigens, and are rapidly cleared without necessitating inflammation [101-102]. Although the mechanisms enabling this efficient clearance in the absence of inflammation have proven difficult to elucidate, recent efforts have been made to characterize the signaling interactions between apoptotic cells and the innate immune system. [103-107]. Until recently, such studies have necessitated reliance on traditional imaging modalities including fluorescence microscopy and flow cytometry. While these techniques continue to yield valuable information, there remains a distinct need for a high-throughput, unbiased, quantitative assay to study signaling between cells and among different cell types. In this work, PC biosensors are incorporated to develop a set of assays that can quickly and broadly screen for cell-cell interactions in the absence of antibodies, stains, or fluorescent dyes while maintaining quantitative sensitivity toward specific apoptotic recognition.

Photonic crystal biosensors have recently been demonstrated in the label-free study of biomolecular binding interactions as well as in cell viability studies in context with prospective anti-cancer drug candidates [67, 108-109]. In this work, the first use of PC biosensor technology to detect specific signaling interactions between multiple cell types is described. Briefly, the biosensor is comprised of a periodic arrangement of dielectric material that effectively prevents propagation of light at specific wavelengths and directions [71]. When illuminated with white light, appropriately configured PCs can reflect narrow band of wavelengths directly dependent on the local density of adsorbed biomolecules or cells [108, 110]. Specifically, the association of cells with the sensor surface modulates the peak wavelength value (PWV) of the reflected light, allowing the detection of binding activity via measurement of a shift in the PWV [111-112]. The resonant reflected light can be detected spectrophotometrically in a microplate-based detection

instrument (BINDTM, SRU Biosystems). When used in context with *in vitro* cell models, the surface and extracellular matrix (ECM) attachment proteins expressed by the cells result in a PWV shift over corresponding regions of the sensor [113].

Previous work has demonstrated that modulation of macrophage response can be achieved upon apoptotic cell recognition [114]. Importantly, this modulation does not require engulfment of the recognized cell by the macrophage. Recent proteomic analysis has shown that the apoptosis results in the association of several classes of proteins with apoptotic membrane vesicles, including signaling enzymes, cytoskeletal and structural proteins, chaperones, and other proteins useful for macromolecular processing. Cellular changes induced by specific apoptotic recognition include morphological alterations within activated cells [115]. In this study, the sensitivity of PC biosensors toward cell attachment modulation was leveraged to detect these morphological changes.

Interactions between apoptotic cells and the innate immune system also have profound implications for tumor immunogenicity. The characteristic lack of immunogenicity displayed by tumour antigens is often attributed to their similarity to self, but this assertion remains ill-equipped to fully explain the limited immunogenic ability of transformed tumour cells. One explanation capable of addressing these concerns is that immune recognition of apoptotic species is capable of modulating the immune response itself. Though this remains but one interesting theory regarding these clinically important findings, the study of such relationships between cells remains hampered by the complexity and indirect nature of currently used techniques.

Previously, *in vitro* evaluations of tumour-host interactions required complex instrumentation and several surface markers to verify viability, activation, and function of individual components of the immune system. A common strategy is to use a proliferative marker such as carboxyfluorescein diacetate (CFDA) in combination with activation techniques such as luciferase reporter assays. Briefly, apoptotic or viable CFDA-stained cells can be

introduced to macrophages tracked with an NF-kB-dependent reporter construct to assay for specific apoptotic recognition. While these and similar approaches have contributed much toward our understanding of immune function, they are limited in scalability and transferability. The study of tumor immunogenicity is further complicated by the fact that studying these interactions in context with combinations of drug candidates can considerably increase the given scale of a study. For these reasons, this work introduces new methods to screen for and study these and other interesting cell-cell interactions.

## 3.2 PC Biosensor Instrumentation and Fabrication

*PCEM Instrumentation*

The detection system used in this study is a modified upright fluorescence microscope, and has been previously described [116]. Briefly, laser light is passed through a rotating diffuser and then collimated by a beam expander. This sequence of optical components results in a spatially uniform, highly collimated beam that is then incident on a high-resolution motorized gimbal-mounted mirror, thus providing collimated illumination at a user-selectable incident angle. In order to maintain a constant illumination area on the device, the gimbal-mounted mirror sits on top of a motorized linear stage that translates laterally as the mirror rotates. As the collimated light at a fixed wavelength is incident on the PC surface, the angle of incidence can be tuned to allow the laser to couple with the PC resonance, thereby allowing maximum field coupling into the transverse magnetic (TM) mode of the PC. The excitation illumination was TM polarized by passing the laser light through a half-wave plate.

*PC Biosensor Fabrication*

Fabrication of the device was performed using a plastic-based nanoreplica molding process [71]. Briefly, a silicon wafer with a negative surface volume image of the desired grating pattern was fabricated using deep-UV lithography and reactive ion etching. A liquid that contains an uncured monomer and a UV-activated polymerization initiator is sandwiched between a flexible plastic sheet and the silicon master wafer to enable the liquid to fill the silicon surface structure subsequent to curing with a high intensity UV lamp (Xenon, Inc). The hardened polymer grating preferentially adheres to the plastic substrate, and thus can be easily peeled away from the silicon. After the molding step, the replica was cut and attached to a 1 × 3 in2 microscope slide. An evaporated SiO2 intermediate layer, ($t_{SiO2}$)= 200 nm, (e-beam evaporation, Denton Inc.) was deposited on the grating surface to control the resonant peak width. After the SiO2 deposition,

~80 nm of TiO2 was deposited by RF sputtering (PVD 75, Kurt Lesker) using an *in-situ* process monitor to accurately achieve a resonance condition that nominally results in λ=633 nm wavelength resonantly coupling to the PC surface at an incident angle of 1° in an aqueous environment. The device is then bonded to PDMS (Sylgard-184, Dow Chemical Company) wells by UV-crosslinking.

## 3.3 Materials and Methods

Cell culture media were obtained from the Cell Media Facility at the University of Illinois at Urbana-Champaign. HEK-clonally derived responder cells (B2.1) were cultured in Dulbecco's modified Eagle's medium (DMEM) with 10% (v/v) fetal bovine serum (FBS), 2 mM L-glutamine and penicillin-streptomycin. S49 murine thymoma cells and Jurkat human T leukemia cells were cultured in RPMI 1640 medium with 10% (v/v) fetal bovine serum (FBS), 2mM L-glutamine, and 50uM 2-mercaptoethanol.

Adherent cell lines were grown in an incubator at 37°C and 5% CO2 until 85% confluence and then passed using trypsin (0.25% + EDTA, Thermo Scientific) every 2-5 days as necessary. For PCEM imaging experiments, B2.1 responder cells were plated on PC biosensors in a total volume of 50 ml at a density of 4-6 x 104 cells/mL. Cell counting was performed with a hemacytometer (Reichert).

*Statistical Analysis*

Two-tailed student's *t* tests were performed for the results described in Fig. 15-16 with $p < 0.05$ used to signify statistical significance. All *p* value determinations were two-tailed. GraphPad software (LaJolla, CA) was used for all calculations concerning statistical evaluation. Unless otherwise noted, error bars indicate one standard error of the mean in either direction.

## 3.4 PC Biosensor Detection of Cell-Cell Signaling Interactions

Previous work has demonstrated that PC biosensors can be used to detect cell attachment in a specific, predictable, and reproducible manner [111, 117]. Briefly, studies have shown that PC biosensors functionalized with anti-CD3, anti-CD28, and anti-CD45 antibodies are capable of resolving specific cell adhesion by cells expressing the corresponding surface markers [67]. Here, a discussion takes place regarding the investigation of the sensitivity of PC biosensors to physiologic changes in cell attachment. Specifically, the study is concerned with the morphological and structural changes that occur in macrophages and non-professional phagocytes ("responders") in the course of recognizing apoptotic "target" cells. Because these changes result in alterations in cell morphology, it was hypothesized that PWV shifts could be detected as a result of changing attachment protein concentration, density, and distribution at the cellular level. To test this prediction, an examination wan conducted regarding the interaction of macrophages and non-professional phagocytes cultured on PC biosensors with distinct suspensions of apoptotic target cells, with addition of viable cells serving as a negative control.

*Label-Free Detection of Specific Apoptotic Recognition*

Transformed human epithelial cells (B2.1, an HEK-derived reporter clone) were cultured overnight on PC biosensor microwell plates (BINDTM, SRU Biosystems) which were then measured for PWV shift resulting from B2.1 ("responder") cell attachment (Figure 14). Viable or apoptotic murine T cells (S49, "targets") were then added several target:responder ratios. As responder cells are cultured at a density sufficient to create a confluent monolayer on the bottom of each microplate well, recognition of the target cells by the responders was monitored in real-time using the BIND Reader Turbo microplate reader, without removal of excess cells.

To confirm the ability of the PC biosensor assay to detect specific apoptotic recognition, the assay described above was repeated with a second target cell type, Jurkat T cells. B2.1 cells were again cultured overnight as responder cells, and measured for PWV shift prior to exposure to viable (open) and apoptotic (black) Jurkat T cells. As an additional negative control, the viable (stippled) and apoptotic (shaded) suspension Jurkat T cells were added to PC biosensor microplate wells that had not been seeded with responder cells (Fig. 15). Consistent with the B2.1-S49 experiment, PWV shift for responder cell attachment was 1.200 ± 0.03nm. The PWV shift upon addition of the Jurkat T cell targets was also on the same order, although markedly more consistent and homogeneous within each ratio. The increased consistency within each treatment group allows for facile distinction between experimental target:responder ratios. This indicates that the label-free detection of responder cell activity and stuructural and morphological change is dose-dependent, owing to the increased frequency of responder cell activity in the presence of increased concentrations of target cells. As expected, apoptotic and viable Jurkat T cells produced minimal PWV shift, with the exception of the highest concentration of apoptotic Jurkat T cells.

*High-Throughput Screening for Apoptotic Immune Interactions*

To provide insight as to the kinetics of signaling interactions between cells, the high-throughput instrument can provide measurements for a 96-well microplate with a temporal resolution of < 15 s. The B2.1-Jurkat target:responder experiment described in Figure 15 was repeated in an effort to (1) identify whether kinetic information would yield any additional insight as to the timeline of specific apoptotic recognition and the corresponding cellular changes and to (2) optimize the experimental protocol for high spatial resolution studies to be performed on PC biosensors using Photonic Crystal Enhanced Microscopy. For this experiment, PWV shift data were collected for the entire microwell plate every 30 s, allowing a complete picture of the cellular attachment density changes elicited by specific apoptotic recognition. Furthermore, this

temporal resolution enables comparison of different treatment scenarios and combinations to be conducted effectively in real-time.

To simplify presentation and explanation, data collected in the kinetic experiment are plotted across three panels in Figure 16, and only every tenth data point is displayed. Figure 16A depicts raw PWV shift values resulting from target addition to responder cells for the highest (10:1) target:responder ratio used in the experiment. Notably, it is possible to distinguish between responders that remain untreated (shaded circles), responders that were treated with viable targets (open triangles), and responders that were exposed to apoptotic targets (closed squares). Because temperature changes and solvent loss can influence PWV shift over extended time periods, PWV shift data were normalized from all samples to the samples to which no target cells were added. This minimizes the influence of environmental considerations on the outcome of the experiment, attempting to control for solvent loss, temperature fluctuations, air movement, and vibrational noise. Normalization was performed by subtracting the PWV shift of responder cells exposed to media in the absence of target cells from the PWV shift of responder cells exposed to media with viable (Fig. 16B) or apoptotic (Fig. 16C) cells for each time point. Examination of the raw data (Fig. 16A) shows that the differences in PWV corresponding to cell attachment density between various treatments are maximized at approximately 30 minutes after target addition. Conversely, the dilution of targets bears little effect on the magnitude of PWV shift in the case of viable responders, all three dilutions of which appear to give PWV shift values within 1 S.E.M. of one another (Fig. 16B). Reconciling this with the normalized results, the PWV shift differences are again maximized 30 minutes post-target addition (Fig. 16C).

*Microscopic Label-Free Analysis of Cell Attachment Density*

To visualize attachment density changes on the scale of individual cells, photonic crystal enhanced microscopy (PCEM) was employed, described previously [116]. In lieu of broadband

white light illuminating the PC biosensor at a fixed angle as in the high-throughput experiments described above, the photonic crystal enhanced microscope relies on a fixed wavelength HeNe light source and a variable-angle translational stage, which allows the user to scan a sample across a range of angles of illumination to find the angle of minimum transmission (AMT) for a given sensor region. Taking advantage of similar photonic crystal biosensors, the instrumentation for PCEM relies upon changes in the AMT rather than a peak wavelength value. As the physical density of cell attachment increases, the AMT for the corresponding sensor region increases proportionally. In this fashion, PCEM instrumentation allows the user to examine changes in cell attachment density for individual cells, and to track those cells as they respond to treatment at a temporal resolution on the order of one frame per minute. While this precludes the possibility of real-time imaging of cell attachment at such high spatial resolution, it is possible to gather data from a series of samples if the experiment is informed by previous study with a higher throughput system, as performed in this work.

Responder (B2.1) cells were plated in 10mm-diameter PDMS wells affixed to PC biosensors configured for PCEM. After overnight culture at 37ºC, the sensors were allowed to come to RT before obtaining post-responder cell attachment images (Fig. 17, 0 min). To minimize the effect of temperature on experimental outcomes, the remaining experimental steps were carried out at RT. After obtaining responder cell attachment images via PCEM, viable and apoptotic target cells were added to the responders at 1:10 and 1:1 target:responder ratios. Lower target:responder ratios were used for these experiments (in comparison to the high-throughput experiments discussed earlier) because floating cellular debris and unbound targets interfered with image acquisition using the high resolution PCEM instruementation. Namely, because the angle scans take 30-60 s to complete, debris floating through the field of interest can obstruct the CCD and prevent capture of high-fidelity cell attachment imagery. As highlighted Fig. 17, particular responder cells treated with apoptotic target cells showed pronounced increases in cell attachment density in the group exposed to apoptotic cells (left,

pink arrows). Notably, cells in both apoptotic target:responder ratios were found to exhibit increases in cell attachment density, while responders treated with viable targets (right) maintained minimal AMT shift for both target:responder ratios. Additionally, a few examples of cells decreasing their attachment strength could be found in both treatment groups at both target:responder ratios.

To demonstrate the quantitative capacity of PCEM for the characterization of apoptotic recognition, localized AMT measurements were made for each of the treatment groups described above. Briefly, cells were measured for AMT shift values w. r. t. background both before (Fig. 18A) and after (Fig. 18B) exposure to viable and apoptotic targets. These measurements were performed for both target:responder ratios, and then categorized and displayed in Figure 18. To exclude the possibility that heterogeneous background readings could influence interpretation of PCEM results, localized background measurements were performed for each cell, selecting a background area of ~100 pixels within 5 microns of the cell border as determined using brightfield images. Intracellular regions were chosen again using ~100-pixel areas within the cell body. The same cells were tracked for pre- and post-target addition measurements, so the net AMT shift resulting from target addition was calculated by comparing the difference between the two measurements for each cell type (Fig. 18C).

Comparison of the resulting measurements shows significant distinction between changes in B2.1 responder cell attachment density upon addition of apoptotic vs. viable Jurkat T cell targets. These data agree with assertions that components of innate immunity are activated by the presentation of recognition determinants on the apoptotic cell surface. The use of PC biosensors to identify individual cells responding to apoptotic target recognition allows an additional vantage point from which to study these interesting interactions, and potentially allows the user to identify them without the need for specific markers, labels, or stains.

## 3.5 Discussion

This work demonstrates the first unbiased, quantitative method for assessing apoptotic recognition on a flexible, high-throughput capable screening platform. The use of photonic crystal biosensors throughout this work allows such screening experiments to be designed with scalability and cost-effectiveness in mind. Furthermore, use of PCEM imaging to identify single cells undergoing specific apoptotic recognition represents the earliest known detection in the absence of fluorescent labels, presenting the possibility of real-time, label-free screening for cell-cell signaling events. Label-free imaging techniques have the added advantage of providing this insight without the use of potentially interfering or cytotoxic stains, fluorophores, or fixative, allowing the possibility of continuous screening throughout the course of cell culture. This also represents the first documented report of applying label-free biosensors for the detection of cellular signaling between multiple cell types *in vitro*. Using inexpensively fabricated devices that are uniform over microplate- and microscope slide-sized sensors allows the possibility of large-scale screening for cell-cell signaling interactions for complex biological systems including apoptotic immunity, tumor immunogenicity, and inflammation.

## 3.6 Figures

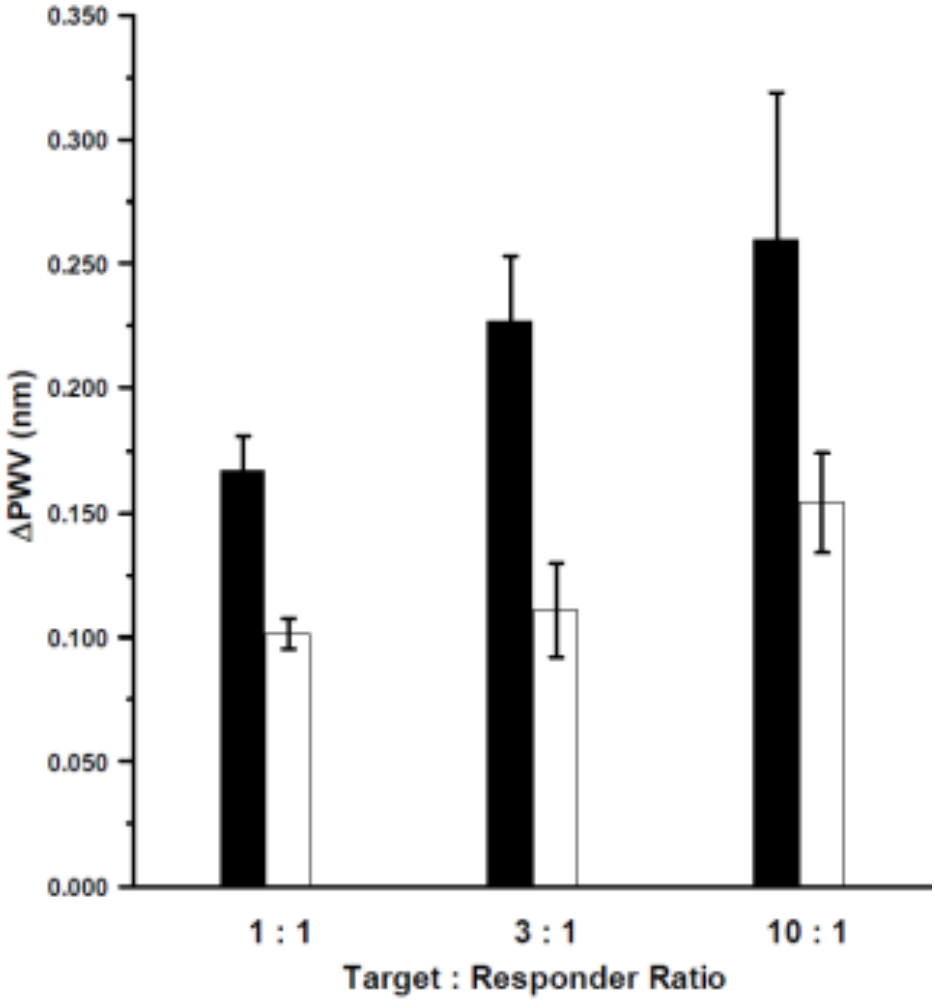


**Figure 14:** An initial PWV shift associated with the attachment of B2.1 cells to the biosensor was recorded (ΔPWV = 1.094 ± 0.128 nm S.E.M.). Viable or apoptotic murine T cells (S49, "targets") were then added to the adherent B2.1 cells ("responders") at several target:responder ratios. Target recognition was detected as a second PWV shift; data for this second PWV shift are presented for apoptotic (■) cells and viable (□) targets. Error bars indicate 1 S.D. in either direction.

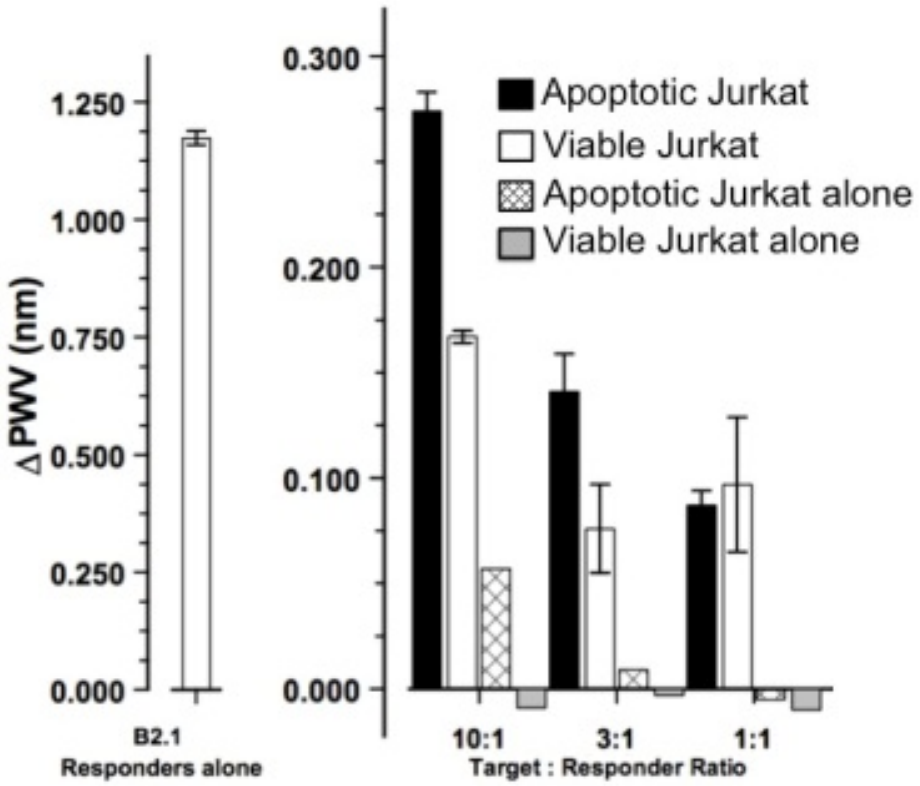


**Figure 15:** An initial PWV shift associated with the attachment of B2.1 cells to the biosensor was measured on the high-throughput PC biosensor system (left), after which viable or apoptotic Jurkat T cells ("targets") were added to the B2.1 cells ("responders") at several ratios. Error bars indicate 1 S.D. in either direction.

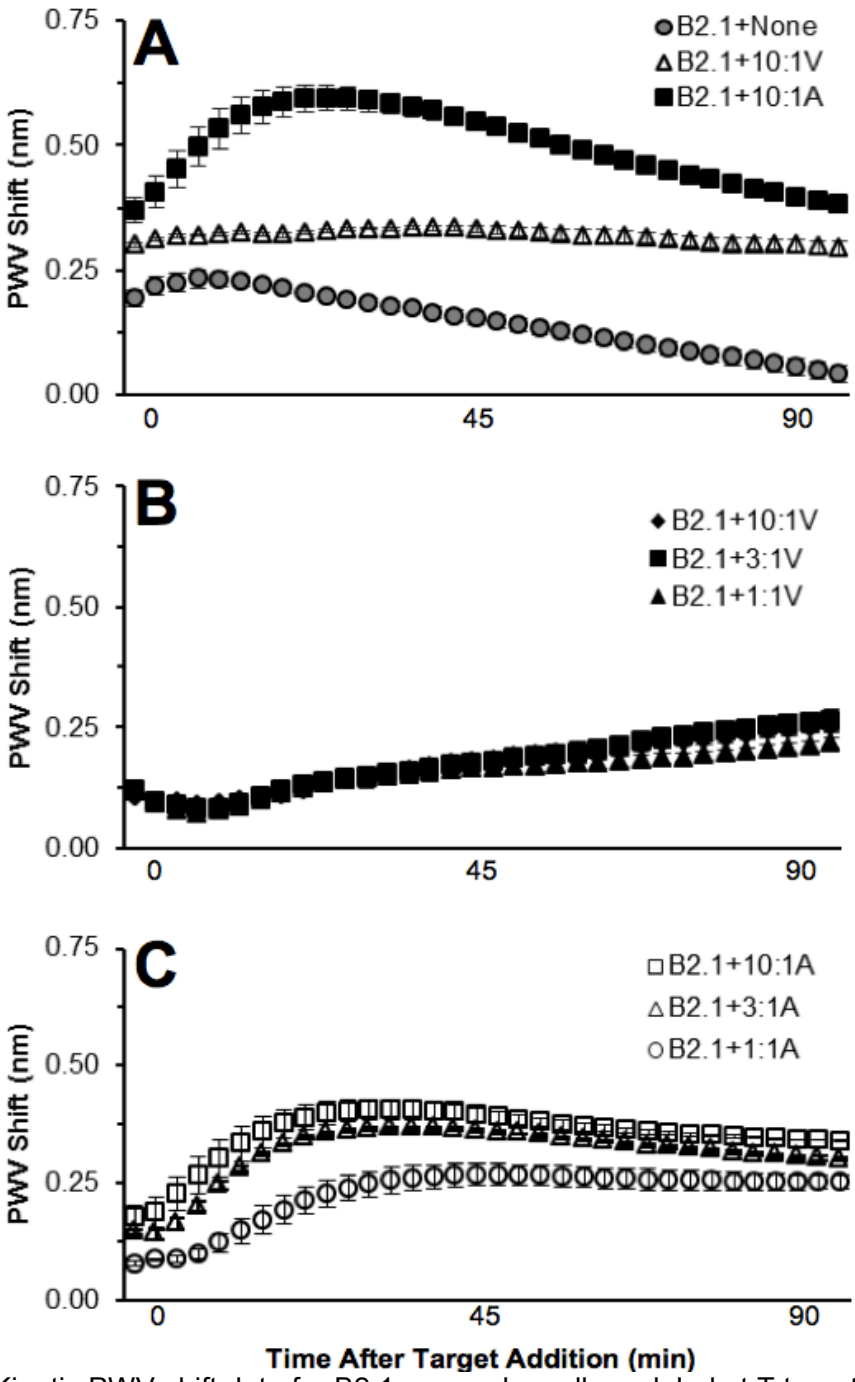


**Figure 16:** Kinetic PWV shift data for B2.1 responder cells and Jurkat T target cells, recorded at 30-s intervals (every tenth read plotted) over 90 min after addition of targets to responders. Responders were cultured on 96-well PC biosensor microplates overnight at 37ºC prior to acquisition of a baseline responder PWV shift read and subsequent target addition, documented here. 3A: Raw PWV shift data for 10:1 viable and apoptotic target:responder ratios show that PWV shift can be used to distinguish between addition of viable targets, apoptotic targets, or medium alone. 3B: PWV shift data for viable target addition are plotted after normalization w. r. t. B2.1 + None values for each time point. 3C: PWV shift data for apoptotic target addition are plotted after normalization w. r. t. B2.1 + None values for each time point. Error bars denote 1 S.E.M. in either direction.

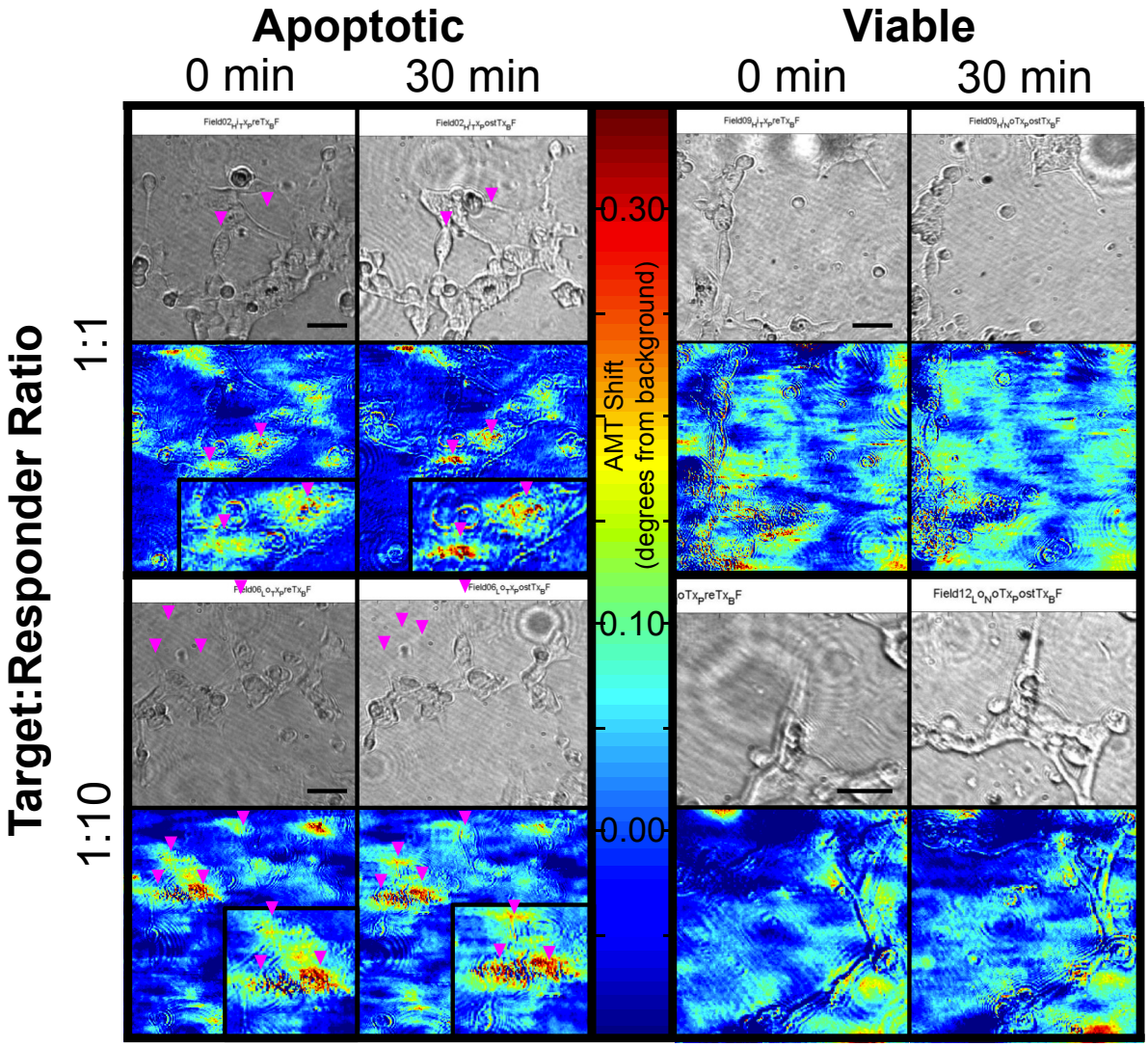


**Figure 17:** Cell attachment density images recorded via PCEM, 30 min after B2.1 responder cells were exposed to apoptotic or viable targets. Bright field images (grayscale) represent bright field information, showing cell structure and morphology. PCEM data (heatmap) show elevated AMT shift w. r. t. background across areas of the sensor over which cell attachment has caused increases in mass density. As highlighted by the pink arrows and insets, certain cells show pronounced increases in cell attachment density, presumably from specific apoptotic recognition in response to Jurkat target cells. Scale bars represent 50 microns. Images were obtained using a 20X microscope objective over a 400x400-micron field of view, and were subsequently cropped and enlarged to enhance detailed comparison.

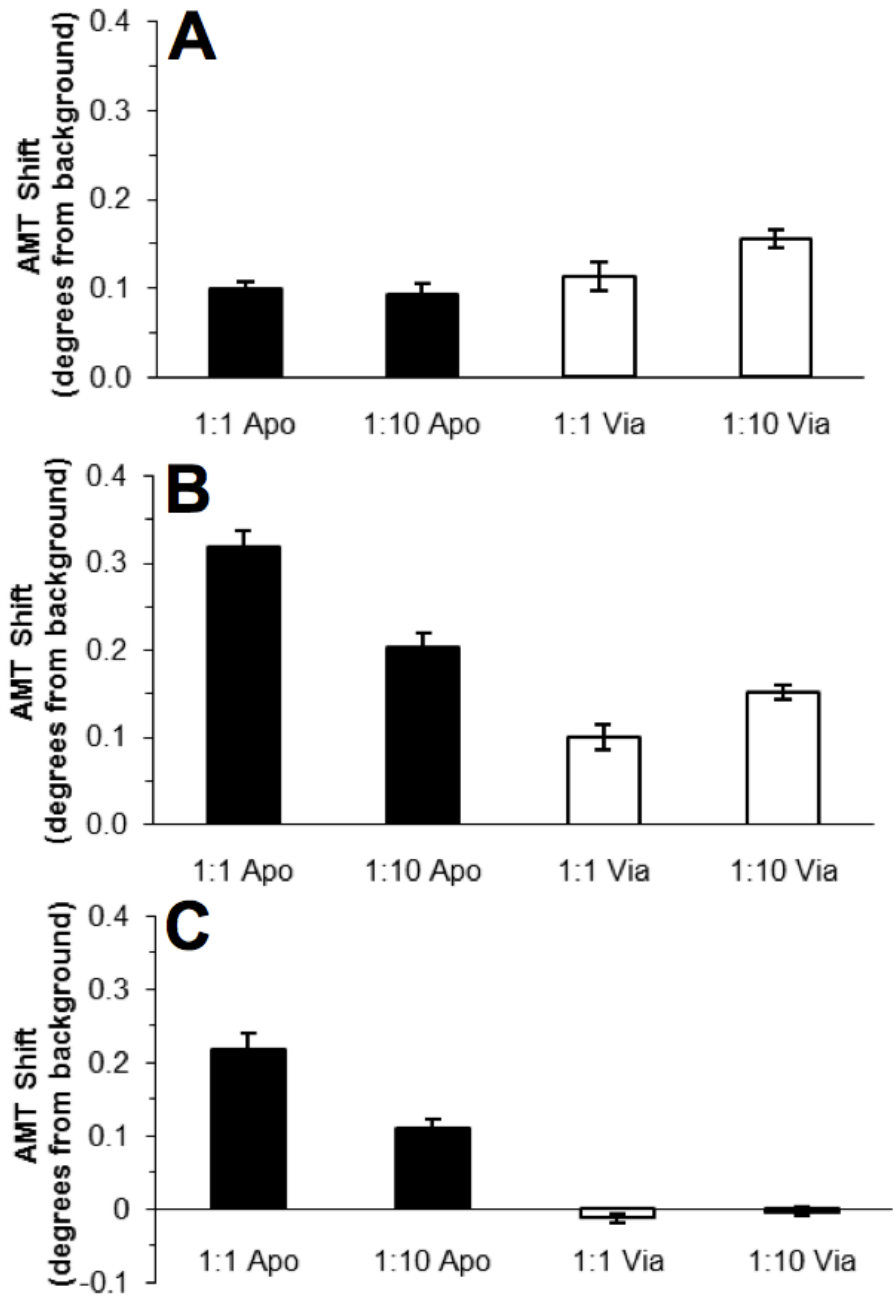


**Figure 18:** Quantification of cell attachment density data collected for B2.1 Responder cells exposed to viable (open bars) and apoptotic (closed bars) at 1:1 and 1:10 target:responder ratios. 5A: Individual cells were measured for mean AMT shift w. r. t. background AMT to assess the initial heterogeneity of the experimental population. 5B: After 30 min exposure to target cells, cell attachment density data were collected for the same cells in each treatment group. 5C: To ease comparison, net AMT shift values were calculated by subtracting the pre-target addition AMT shift values from the corresponding post-target addition AMT shift values. The resulting net AMT shift indicates the relative increase in cell attachment density due to responder cell activity in the presence of apoptotic or viable target cells. Values displayed are for *n*=9, *n*=12, *n*=11, and *n*=13 for 1:1 apoptotic, 1:10 apoptotic, 1:1 viable, and 1:10 viable target:responder ratios, respectively. P-values for net AMT shifts were 6.12x10^-7 and 4.60x10^-8 for 1:1 and 1:10 target:responder ratios, respectively.

# REFERENCES


1. J. E. Sulston, H.R. Horvitz, “Post-embryonic cell lineages of the nematode, Caenorhabdis elegans, ” Dev. Biol. 56(1):110-56, 1977.

2. Kimble J., Hirsh D. The postembryonic cell lineages of the hermaphrodite and male gonads in Caenorhabdis elegans. Dev. Biol. 70(2):396-417.

3. D. Wirtz, K. Konstantopoulos and P. C. Searson, "The physics of cancer: the role of physical interactions and mechanical forces in metastasis," *Nat. Rev. Cancer.,* vol. 11, pp. 512-522, Jun 24, 2011.

4. N. J. Boudreau and P. L. Jones, "Extracellular matrix and integrin signalling: the shape of things to come," *Biochem. J.,* vol. 339 ( Pt 3), pp. 481-488, May 1, 1999.

5. M. Barczyk, S. Carracedo and D. Gullberg, "Integrins," *Cell Tissue Res.,* vol. 339, pp. 269-280, Jan, 2010.

6. T. D. Palmer, W. J. Ashby, J. D. Lewis and A. Zijlstra, "Targeting tumor cell motility to prevent metastasis," *Adv. Drug Deliv. Rev.,* vol. 63, pp. 568-581, Jul 18, 2011.

7. J. P. Higgins, M. B. Bernstein and J. W. Hodge, "Enhancing immune responses to tumor-associated antigens," *Cancer. Biol. Ther.,* vol. 8, pp. 1440-1449, Aug, 2009.

8. N. Makrilia, A. Kollias, L. Manolopoulos and K. Syrigos, "Cell adhesion molecules: role and clinical significance in cancer," *Cancer Invest.,* vol. 27, pp. 1023-1037, Dec, 2009.

9. E. Voronov, E. Reich, S. Dotan, P. Dransh, I. Cohen, M. Huszar, M. Fogel, H. K. Kleinman, R. M. White and R. N. Apte, "Effects of IL-1 molecules on growth patterns of 3-MCA-induced cell lines: an interplay between immunogenicity and invasive potential," *J. Immunotoxicol.,* vol. 7, pp. 27-38, Mar, 2010.

10. A. Jemal, R. Siegel, J. Xu and E. Ward, "Cancer statistics, 2010," *CA Cancer. J. Clin.,* vol. 60, pp. 277-300, Sep-Oct, 2010.

11. B. Weigelt, J. L. Peterse and L. J. van 't Veer, "Breast cancer metastasis: markers and models," *Nat. Rev. Cancer.,* vol. 5, pp. 591-602, Aug, 2005.

12. Robbins SL, Kumar Vinay, Cotran RS. Robbins and Cotran Pathologic Basis of Disease, 8$^{th}$ed. Copyright 2010, Saunders, Philadelphia PA.

13. Thiery J., Sleeman J., “Complex networks orchestrate epithelial-mesenchymal transition,” *Nat. Rev. Mol. Cell Biol.,* 7(2):131-142.

14. Robert D. Schreiber,1 and Mark J. Smyth2,3 Matthew D. Vesely,1 Michael H. Kershaw,2,3,4 Natural Innate and Adaptive immunity to Cancer

15. Dighe AS, Richards E, Old LJ, Schreiber RD. 1994. Enhanced in vivo growth and resistance to rejection of tumor cells expressing dominant negative IFN γreceptors. *Immunity* 1:447–56

16. Kaplan DH, Shankaran V, Dighe AS, Stockert E, Aguet M, et al. 1998. Demonstration of an interferon γ-dependent tumor surveillance system in immunocompetent mice. *Proc. Natl. Acad. Sci. USA* 95:7556–61

17. Engel AM, Svane IM, Mouritsen S, Rygaard J, Clausen J, Werdelin O. 1996. Methylcholanthreneinduced sarcomas in nude mice have short induction times and relatively low levels of surfaceMHCclass I expression. *APMIS* 104:629–39

18. Engel AM, Svane IM, Rygaard J, Werdelin O. 1997. MCA sarcomas induced in scid mice are more immunogenic than MCA sarcomas induced in congenic, immunocompetent mice. *Scand. J. Immunol* 45:463–70

19. Shankaran V, Ikeda H, Bruce AT, White JM, Swanson PE, et al. 2001. IFNγ and lymphocytes prevent primary tumour development and shape tumour immunogenicity. *Nature* 410:1107–11

20. Dunn, Old, and Schreiber 2004

21. Koebel, Vermi, Swann 2007

22. P. Boyle, B. Levin, International Agency for Research on Cancer and World Health Organization, *World Cancer Report 2008.* Lyon; Geneva: International Agency for Research on Cancer; Distributed by WHO Press, 2008.

23. L. Starita, "The multiple nuclear functions of BRCA1: transcription, ubiquitination and DNA repair," *Curr. Opin. Cell Biol.,* vol. 15, pp. 345 <last_page> 350, 2003.

24. P. C. Walsh, "Chemoprevention of prostate cancer," *N. Engl. J. Med.,* vol. 362, pp. 1237-1238, Apr 1, 2010.

25. J. Hall, M. Lee, B. Newman, J. Morrow, L. Anderson, B. Huey and M. King, "Linkage of early-onset familial breast cancer to chromosome 17q21" *Science,* vol. 250, pp. 1684 <last_page> 1689, 1990.

26. D. J. Schaid, "The complex genetic epidemiology of prostate cancer," *Hum. Mol. Genet.,* vol. 13 Spec No 1, pp. R103-21, Apr 1, 2004.

27. N. Bardeesy and R. A. DePinho, "Pancreatic cancer biology and genetics " *Nat. Rev. Cancer.,* vol. 2, pp. 897-909, Dec, 2002.

28. C. D. Rogers, F. J. Couch, K. Brune, S. T. Martin, J. Philips, K. M. Murphy, G. Petersen, C. J. Yeo, R. H. Hruban and M. Goggins, "Genetics of the FANCA gene in familial pancreatic cancer " *J. Med. Genet.,* vol. 41, pp. e126, Dec, 2004.

29. S. Yachida and C. A. Iacobuzio-Donahue, "The pathology and genetics of metastatic pancreatic cancer " *Arch. Pathol. Lab. Med.,* vol. 133, pp. 413-422, Mar, 2009.

30. P. Panorchan, M. S. Thompson, K. J. Davis, Y. Tseng, K. Konstantopoulos and D. Wirtz, "Single-molecule analysis of cadherin-mediated cell-cell adhesion " *J. Cell. Sci.,* vol. 119, pp. 66-74, Jan 1, 2006.

31. F. Li, S. Redick, H. Erickson and V. Moy, "Force Measurements of the a5ß1 Integrin–Fibronectin Interaction," *Biophys. J.,* vol. 84, pp. 1252-1262, 2003.

32. S. Bajpai, Y. Feng, R. Krishnamurthy, G. D. Longmore and D. Wirtz, "Loss of alpha-catenin decreases the strength of single E-cadherin bonds between human cancer cells " *J. Biol. Chem.,* vol. 284, pp. 18252-18259, Jul 3, 2009.

33. M. E. Berginski, E. A. Vitriol, K. M. Hahn and S. M. Gomez, "High-resolution quantification of focal adhesion spatiotemporal dynamics in living cells," *PLoS One,* vol. 6, pp. e22025, 2011.

34. A. Dovas, B. Gligorijevic, X. Chen, D. Entenberg, J. Condeelis and D. Cox, "Visualization of actin polymerization in invasive structures of macrophages and carcinoma cells using photoconvertible beta-actin-Dendra2 fusion proteins " *PLoS One,* vol. 6, pp. e16485, Feb 14, 2011.

35. J. Guck, S. Schinkinger, B. Lincoln, F. Wottawah, S. Ebert, M. Romeyke, D. Lenz, H. M. Erickson, R. Ananthakrishnan, D. Mitchell, J. Kas, S. Ulvick and C. Bilby, "Optical deformability as an inherent cell marker for testing malignant transformation and metastatic competence " *Biophys. J.,* vol. 88, pp. 3689-3698, May, 2005.

36. A. Rahman, Y. Tseng and D. Wirtz, "Micromechanical coupling between cell surface receptors and RGD peptides" *Biochem. Biophys. Res. Commun.,* vol. 296, pp. 771-778, 2002.

37. D. C. Worth and M. Parsons, "Advances in imaging cell-matrix adhesions," *J. Cell. Sci.,* vol. 123, pp. 3629-3638, Nov 1, 2010.

38. S. M. Shamah and B. T. Cunningham. Label-free cell-based assays using photonic crystal optical biosensors *Analyst* 2011.

39. A. W. Peterson, M. Halter, A. Tona, K. Bhadriraju and A. L. Plant. Using surface plasmon resonance imaging to probe dynamic interactions between cells and extracellular matrix *Cytometry A.* 2010.

40. C. L. Chaffer and R. A. Weinberg, "A perspective on cancer cell metastasis " *Science,* vol. 331, pp. 1559-1564, Mar 25, 2011.

41. T. Borovski, F. De Sousa E Melo, L. Vermeulen and J. P. Medema, "Cancer stem cell niche: the place to be " *Cancer Res.,* vol. 71, pp. 634-639, Feb 1, 2011.

42. M. Mego, S. A. Mani and M. Cristofanilli, "Molecular mechanisms of metastasis in breast cancer--clinical applications " *Nat. Rev. Clin. Oncol.,* vol. 7, pp. 693-701, Dec, 2010.

43. Ucker, David S., "Phagocytosis of Dying Cells: From Molecular Mechanisms to Human Diseases; Innate Apoptotic Immunity: A Potent Immunosuppressive Response Repertoire Elicited by Specific Apoptotic Cell Recognition " pp. 163-187, 2009.

44. F. M. Watt, "Out of Eden: Stem Cells and Their Niches " *Science,* vol. 287, pp. 1427 - 1430, 2000.

45. S. M. Dellatore, A. S. Garcia and W. M. Miller, "Mimicking stem cell niches to increase stem cell expansion " *Curr. Opin. Biotechnol.,* vol. 19, pp. 534-540, Oct, 2008.

46. K. A. Moore, "Recent advances in defining the hematopoietic stem cell niche " *Curr. Opin. Hematol.,* vol. 11, pp. 107-111, Mar, 2004.

47. Wang 2011 Impedance Imaging

48. S. Lofas, "Dextran modified self-assembled monolayer surfaces for use in biointeraction analysis with surface plasmon resonance " 1995.

49. G. J. Ciambrone, V. F. Liu, D. C. Lin, R. P. McGuinness, G. K. Leung and S. Pitchford, "Cellular dielectric spectroscopy: a powerful new approach to label-free cellular analysis " *J. Biomol. Screen.,* vol. 9, pp. 467-480, Sep, 2004.

50. U. Jonsson, L. Fagerstam, B. Ivarsson, B. Johnsson, R. Karlsson, K. Lundh, S. Lofas, B. Persson, H. Roos and I. Ronnberg, "Real-time biospecific interaction analysis using surface plasmon resonance and a sensor chip technology," *BioTechniques,* vol. 11, pp. 620-627, Nov, 1991.

51. A. M. Giannetti, B. D. Koch, and M. F. Browner, "Surface Plasmon Resonance Based Assay for the Detection and Characterization of Promiscuous Inhibitors," J. Med. Chem., vol. 51, pp. 574-580, 2008.

52. B. Liedberg, C. Nylander, I. Lundström, “Surface plasmon resonance gas detection and biosensing,” Sensors and Actuators, 4 (1983), pp. 299–304

53. C. Nylander, B. Liedberg, T. Lind. “Gas detection by means of surface plasmon resonance,” Sensors and Actuators, 3 (1982), pp. 79–88

54. M.M.B. Vidal, R. Lopez, S. Aleggret, J. Alonso-Chamarro, I. Garces, J. Mateo Determination of probable alcohol yield in musts by means of an SPR optical sensor. Sensors and Actuators B, 11 (1993), pp. 455–459

55. J. Homola1, a, , Sinclair S. Yeea, Günter Gauglitzb Surface plasmon resonance sensors: review. Sensors and Actuators B: Chemical 54:1-2 (1999), pp.3-15

56. E. M. Yeatman and E. A. Ash, “Surface plasmon microscopy,” Electron. Lett. 23(20), pp.1091-1092.

57. E.M. Yeatman and E. A. Ash, “Surface plasmon scanning microscopy”, Proc. SPIE 897, pp.100-325 (1988)

58. B. Rothenhauser and W. Knoll, “Surface-plasmon microscopy,” *Nature* 332 pp. 615 – 617, 1988.

59. D. G. Myszyka, "Improving biosensor analysis," *Journal of Molecular Recognition*, vol. 12, pp. 279-284, 1999.

60. G. A. Papalia, S. Leavitt, M. A. Bynum, P. S. Katsamba, R. Wilton, H. Qiu, M. Steukers, S. Wang, L. Bindu, S. Phogat, A. M. Giannetti, T. E. Ryan, V. A. Pudlak, K. Matusiewicz, K. M. Michelson, A. Nowakowski, A. Pham-Baginski, J. Brooks, B. C. Tieman, B. D. Bruce, M. Vaughn, M. Baksh, Y. H. Cho, M. D. Wit, A. Smets, J. Vandersmissen, L. Michiels, and D. G. Myszka, "Comparative analysis of 10 small molecules binding to carbonic anhydrase II by different investigators using Biacore technology," *Analytical Biochemistry*, vol. 359, pp. 94-105, 2006.

61. E. Katz, I. WIllner, “Probing Biomolecular Interactions at Conductive and Semiconductive Surfaces by Impedance Spectroscopy: Routes to Impedimetric Immunosensors, DNA-Sensors, and Enzyme Biosensors,” *Electroanalysis* 15(11) pp. 913-947, 2003.

62. I. Giaever, C.R. Keese, “Monitoring fibroblast behavior in tissue culture with an applied electric field,” *Proc. Nat. Acad. Sci.* 81 pp. 3761 – 3764, 1984.

63. I. Giaever, C.R. Keese, “A morphological biosensor for mammalian cells,” *Nature* 366, pp.591-592, 1993.

64. W. Wang, K. Foley, X. Shan, S. Wang, S. Eaton, V. J. Nagaraj, P. Wiktor, U. Patel, N. Tao, “Single cells and intracellular processes studied by a plasmonic-based electrochemical impedance microscopy,” *Nature Chemistry* 3 pp. 249-255, 2011.

65. Z. Wang, I. S. Chun, Xiuling Li, Z. Y. Ong, E. Pop, L. Millet, M. Gillette, G. Popescu, “Topography and refractometry of nanostructures using spatial light interference microscopy (SLIM),” Opt. Lett. 35(2) pp. 208-210.

66. Z. Wang, L. Millet, M. Mir, H. Ding, S. Unarunotai, J. Rogers, M. U. Gillette, and G. Popescu, “Spatial light interference microscopy (SLIM)”, Optics Express 19(2) pp. 1016-1026 (2011)

67. B. T. Cunningham, P. Li, S. Schulz, B. Lin, C. Baird, J. Gerstenmaier, C. Genick, F. Wang, E. Fine and L. Laing, "Label-free assays on the BIND system " *J. Biomol. Screen.,* vol. 9, pp. 481-490, 2004.

68. S. M. Shamah and B. T. Cunningham, “Label-free cell-based assays using photonic crystal optical biosensors, “ *Analyst* 136(6) pp. 1090-1102, 2011.

69. S. S. Wang and R. Magnusson, "Theory and applications of guided-mode resonance filters," *Applied Optics,* vol. 32, pp. 2606-2613, 1993.

70. P. C. Mathias, “Improved microarray sensitivity using photonic crystal enhanced fluorescence,”, pp. 27, University of Illinois at Urbana-Champaign, Urbana, IL, 2010.

71. B. Cunningham, P. Li, B. Lin and J. Pepper, "Colorimetric resonant reflection as a direct biochemical assay technique " *Sensors Actuators B: Chem.,* vol. 81, pp. 316 <last_page> 328, 2002.

72. B. Cunningham, B. Lin, J. Qiu, P. Li, J. Pepper and B. Hugh, "A plastic colorimetric resonant optical biosensor for multiparallel detection of label-free biochemical interactions " *Sensors Actuators B: Chem.,* vol. 85, pp. 219 <last_page> 226, 2002.

73. B. T. Cunningham and L. Laing, "Microplate-based, label-free detection of biomolecular interactions: applications in proteomics," *Expert Rev. Proteomics,* vol. 3, pp. 271-281, Jun, 2006.

74. I. Block, P. Mathias, N. Ganesh and S. Jones…, "A detection instrument for enhanced-fluorescence and label-free imaging on photonic crystal surfaces " 2009.

75. N. C. Lindquist, A. Lesuffleur, H. Im and S. H. Oh, "Sub-micron resolution surface plasmon resonance imaging enabled by nanohole arrays with surrounding Bragg mirrors for enhanced sensitivity and isolation " *Lab. Chip,* vol. 9, pp. 382-387, Feb 7, 2009.

76. N. Ganesh, I. D. Block and B. T. Cunningham, "Near ultraviolet-wavelength photonic-crystal biosensor with enhanced surface-to-bulk sensitivity ratio " *Appl. Phys. Lett.,* vol. 89, pp. 023901, 2006.

77. M. J. Smyth, G. P. Dunn, and R. D. Schreiber, "Cancer immunosurveillance and immunoediting: the roles of immunity in suppressing tumor development and shaping tumor immunogenicity," *Adv Immunol.*, 90, pp: 1-50, 2006.

78. I. Marigo, L. Dolcetti, P. Serafini, P. Zanovello and V. Bronte, "Tumor-induced tolerance and immune suppression by myeloid derived suppressor cells," *Immunol. Rev.,* vol. 222, pp. 162-179, Apr, 2008.

79. K. Liu, T. Iyoda, M. Saternus, Y. Kimura, K. Inaba and R. M. Steinman, "Immune Tolerance After Delivery of Dying Cells to Dendritic Cells In Situ " *J. Exp. Med.,* vol. 196, pp. 1091 <last_page> 1097, 2002.

80. L. Stuart, M. Lucas and C. Simpson, "Inhibitory effects of apoptotic cell ingestion upon endotoxin-driven myeloid dendritic cell maturation," 2002.

81. R. Kim, M. Emi, K. Tanabe, and K. Arihiro, "Tumor-Driven Evolution of Immunosuppressive Networks during Malignant Progression," *Cancer Research* 66 pp. 5527-5536, 2006.

82. Somasundaram R, Jacob L, Swoboda R, et al. Inhibition of cytolytic T lymphocyte proliferation by autologous CD4+/CD25+ regulatory T cells in a colorectal carcinoma patient is mediated by transforming growth factor-ß. Cancer Res 2002;62:5267–72.

83. Berger CL, Tigelaar R, Cohen J, et al. Cutaneous T-cell lymphoma: malignant proliferation of T-regulatory cells. Blood 2005;105:1640–7.

84. He X, Stuart JM. Prostaglandin $E_2$ selectively inhibits human CD4+ T cells secreting low amounts of both IL-2 and IL-4. J Immunol 1999;163:6173–9.

85. Gabrilovich D, Ishida T, Oyama T, et al. Vascular endothelial growth factor inhibits the development of dendritic cells and dramatically affects the differentiation of multiple hematopoietic lineages *in vivo*. Blood 1998;92:4150–66.

86. D. H. Munn, M. D. Sharma, J. R. Lee, K. G. Jhaver, T. S. Johnson, D. B. Keskin, B. Marshall, P. Chandler, S. J. Antonia, R. Burgess, Craig L. Slinguff, Andrew L. Mellor, “Potential regulatory function of human dendritic cells expressing indoleamine 2,3-dioxygenase,” Science 2002;297:1867–70.

87. T. R. Cox and J. T. Erler, “Remodeling and homeostasis of the extracellular matrix: implications for fibrotic diseases and cancer,” *Dis. Model. Mech.* 4(2) pp. 165-178, 2011.

88. R. E. Voll, M. Herrmann, E. A. Roth, C. Stach, J. R. Kalden, I. Girkontaite, “Immunosuppressive effects of apoptotic cells,” *Nature* 390, pp. 350-351, 1997.

89. P. Hoffmann, C. Ogden and Y. Leverrier…, "Phosphatidylserine (PS) induces PS receptor–mediated macropinocytosis and promotes clearance of apoptotic cells " 2001.

90. J. E. Mitchell, M. Cvetanovic, N. Tibrewal, V. Patel, O. R. Colamonici, M. O. Li, R. A. Flavell, J. S. Levine, R. B. Birge and D. S. Ucker, "The presumptive phosphatidylserine receptor is dispensable for innate anti-inflammatory recognition and clearance of apoptotic cells " *J. Biol. Chem.,* vol. 281, pp. 5718-5725, Mar 3, 2006.

91. Li, P.Y., Lin, B., Gerstenmaier, J. Cunningham, B.T., "A New Method for Label-Free Imaging of Biomolecular Interactions," *Sens. Act. B* 99:6-13, 2004.

92. Chan, L., Gosangari, S., Watkin, K., Cunningham, B.T., “"A label-free photonic crystal biosensor imaging method for detection of cancer cell cytotoxicity and proliferation," *Apoptosis*, 12(6)1061-1068, 2007.

93. Y. Yanase, T. Hiragun, S. Kaneko, H. J. Gould, M. W. Greaves, M. Hide, “Detection of refractive index changes in individual living cells by means of surface plasmon resonance imaging,” *Biosens Bioelec.* 26 (2010) 674–681, 2010.

94. Bivolarska, M., Velinov, T., Stoitsova, S., “Guided-wave and ellipsometric imaging of supported cells,” *J. Micros.* 224(3)242-248, 2006.

95. Marinkovaa, D., M. Bivolarska, L. Ahtapodov, L. Yotova, R. Mateva, T. Velinov, “Plasmon microscopy and imaging ellipsometry of *Artrobacter oxydans* attaced on polymer films,” *Coll. Surf. B: Biointer.* 65:276–280, 2008.

96. Block, I.D., Mathias, P.C., Jones, S.I., Vodkin, L.O., and Cunningham, B.T., “Optimizing the spatial resolution of photonic crystal label-free imaging,” *App. Optics* 48(34), pp. 6567-6574, 2009.

97. Miskon, A., Ehashi, T., Mahara, A., Uyama, H., Yamaoka, T., “Beating behavior of primary neonatal cardiomyocytes and cardiac-differentiated P19.CL6 cells on different extracellular matrix components,” *J. Artif. Org.* 12(2), pp. 111-117, 2009.

98. A. H. Maass, M. Buvoli, “Cardiomyocyte preparation, culture, and gene transfer,” *Meth. Mol Biol.* 366, pp. 321-30, 2007.

99. T. Huang, , D. He, G. Kleiner, J. Kuluz, “Neuron-like differentiation of adipose-derived stem cells from infant piglets *in vitro*,” *J. Spinal Cord Med.* 30(S1:S35-40), 2007.

100. M. E. Caldwell, E. M. Yeatman, “Surface-plasmon spatial light modulators based on liquid crystal,” *App. Optics* 31(20) pp. 3880-289, 1992.

101. B. A. Cocca, A. M. Cline and M. Z. Radic, "Blebs and apoptotic bodies are B cell autoantigens," *J. Immunol.,* vol. 169, pp. 159-166, Jul 1, 2002.

102. J. F. Kerr, A. H. Wyllie and A. R. Currie, "Apoptosis: a basic biological phenomenon with wide-ranging implications in tissue kinetics," *Br. J. Cancer,* vol. 26, pp. 239-257, Aug, 1972.